NASA
National Aeronautics and
Space Administration

Lyndon B. Johnson Space Center
Houston, Texas 77058

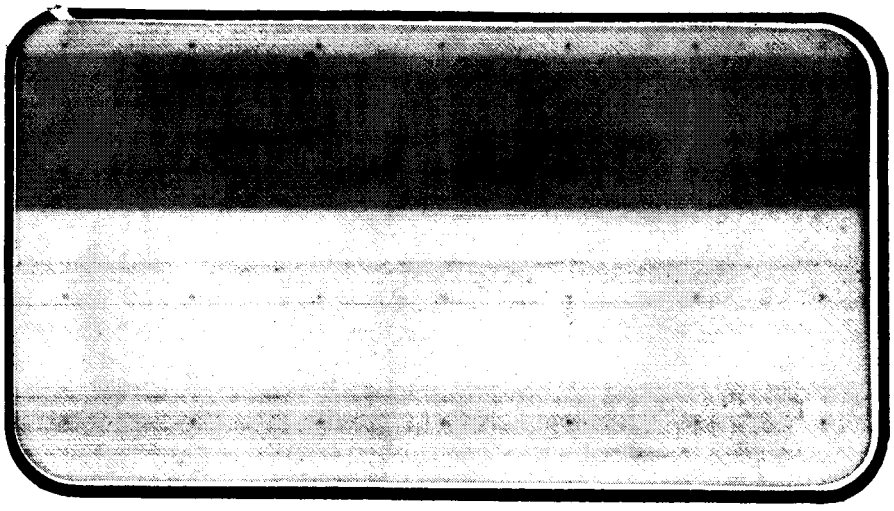

SPACE SHUTTLE AEROTHERMODYNAMIC DATA REPORT

Data Management SERVICES

HUNTSVILLE ELECTRONICS DIVISION CHRYSLER CORPORATION

March 1982

DMS-DR-2490
NASA-CR-167,350

VOLUME 2 OF 3

TEST RESULTS FROM THE NASA/ROCKWELL INTERNATIONAL SPACE SHUTTLE 0.0175-SCALE ORBITER MODELS 56-0/60-0 AND 0.04-SCALE ORBITER FOREBODY MODEL 83-0 CONDUCTED IN THE AEDC/VKF-B 50-INCH HYPERSONIC WIND TUNNEL (TESTS OH109 AND OH109B)

by

J. Gee and J. Nakamoto
Rockwell International STS D&P Division

Prepared under NASA Contract Number NAS9-16283

by

Data Management Services
Chrysler Huntsville Electronics Division
Slidell Engineering Office
New Orleans, Louisiana 70189

for

Engineering Analysis Division

Johnson Space Center
National Aeronautics and Space Administration
Houston, Texas

WIND TUNNEL TEST SPECIFICS:

Test Number:	V41B-G9 or CALSPAN Project No. V41B-13
NASA Series No.:	OH109 and OH109B
Model Nos.:	56-0, 60-0 and 83-0
Test Dates:	October 27 to November 24, 1980
Occupancy Hours:	48.1

FACILITY COORDINATOR:

L. L. Trimmer
Von Karman Gas Dynamics Facility
Arnold Engineering Development Center
Arnold AF Station, TN 37389

Phone: (615) 455-2611, X-7640

PROJECT ENGINEERS:

Jim A. Collins
Jim Gee
Mail Code 41-AC07
Rockwell International
STS D&P Division
12214 Lakewood Blvd.
Downey, California 90241

Phone: (213) 922-5005

Kenneth W. Nutt
VKF/ADP, Mail Stop 400
Calspan Field Services, Inc.
Arnold AFS, TN 37389

Phone: (615) 455-2611, X-575

DATA MANAGEMENT SERVICES:

Prepared by: Liaison -- S. R. Houlihan
Operations - B. J. Burst

Reviewed by: G. W. Klug

Approved: _____
J. L. Glynn, Manager
Data Operations

Concurrence: _____
N. D. Kemp, Manager
Data Management Services

Chrysler Huntsville Electronics Division/Slidell Engineering Office assumes no responsibility for the data presented other than display characteristics.

TEST RESULTS FROM THE NASA/ROCKWELL INTERNATIONAL SPACE SHUTTLE 0.0175-SCALE ORBITER MODELS 56-0/60-0 AND 0.04-SCALE ORBITER FOREBODY MODEL 83-0 CONDUCTED IN THE AEDC/VKF-B 50-INCH HYPERSONIC WIND TUNNEL (TESTS OH109 AND OH109B)

by

J. Gee and J. Nakamoto
Rockwell International STS D&P Division

ABSTRACT

Orbiter Heating Test, OH109, was conducted using scaled Space Shuttle Orbiter models at the Arnold Engineering Development Center's Von Karman Facility (AEDC-VKF) Hypersonic Wind Tunnel B, to obtain additional aerodynamic heating data in finer detail than previously tested for Orbiter STS-1 entry yaw angles. The test program utilized three Rockwell International models: the 0.0175 scale 56-0 and 60-0, and the 0.04 scale 83-0.

Data were recorded at yaw angles of 0, $\pm$0.5, $\pm$1.0 and $\pm$2.0 degrees at angles of attack of 20, 25, 27.5, 30, 32.5, 35, and 40 degrees. Nominal Mach number was 8.0 and Reynolds number (x 10^6/ft) values were 0.5, 1.0, 2.0, 3.0, and 3.7. In addition to the required yaw heating objectives, oil flow tests were conducted on the 83-0 model and the 60-0 model, with elevon deflections of 0 and 5 degrees.

A phase-change paint test was added on to the OH109 test program and designated OH109B. The objective of the phase-change paint test was to establish the peak heating location for the SILTS* pod located on the orbiter vertical tail. This portion of the test was performed on the 56-0 model (See Table VII).

---

*Shuttle Infrared Leeside Temperature Sensor (SILTS)

All the planned aero heating objectives were fulfilled. Two hundred and forty-three (243) data runs were obtained to support the test objectives - 89 for the 60-0 model, 77 for the 83-0 model, and 77 for the 56-0 model.

All oil flow requirements were met with the exception of three test conditions for model 60-0 with elevons at 0 degrees and angle of attach of 40 degrees. These three test conditions were Reynolds number (x 10^6/ft) of 0.5, 1.0, and 2.0.

TABLE OF CONTENTS

INDEX OF MODEL FIGURES

INDEX OF DATA FIGURES

FIGURE NUMBER	TITLE	CONDITIONS VARYING	PLOTTED COEFFICIENTS SCHEDULE	PAGES
60-0 OMS BASIC PLOTS (VOLUME 2 - Microfiche pages 1 through 22)				
1	AERO HEATING ON AFFDL OMS POD, REYNOLDS NUMBER = 3.7 MILLION	BETA, ALPHA, XB/LB SPDBRK	A	1-231
2	AERO HEATING ON AFFEL OMS POD, REYNOLDS NUMBER = 3.0 MILLION	BETA, XB/LB	A	232-275
3	AERO HEATING ON AFFDL OMS POD, REYNOLDS NUMBER = 2.0 MILLION	BETA, ALPHA, XB/LB	A	276-341
4	AERO HEATING ON AFFDL OMS POD, REYNOLDS NUMBER = 1.0 MILLION	BETA, XB/LB	A	342-374
5	AERO HEATING ON AFFDL OMS POD, REYNOLDS NUMBER = 0.5 MILLION	BETA, XB/LB	A	375-385
6	AERO HEATING VS. ALPHA AT VARIOUS LOCATIONS ON AFFDL OMS POD	BETA, ZO, XB/LB	B	386-559
7	AERO HEATING VS. BETA AT VARIOUS LOCATIONS ON AFFDL OMS POD	ALPHA, ZO, XB/LB RN/L	C	560-1342
60-0 OMS BETA EFFECTS (VOLUME 2 - Microfiche pages 23 through 26)				
8	BETA EFFECTS ON AERO HEATING ON THE AFFDL OMS POD	T/C NO, ALPHA RN/L, XB/LB	D	1-220

INDEX OF DATA FIGURES (Continued)

FIGURE NUMBER	TITLE	CONDITIONS VARYING	PLOTTED COEFFICIENTS SCHEDULE	PAGES
	60-0 VERTICAL TAIL BASIC PLOTS (VOLUME 2 - Microfiche pages 27 through 37)			
9	AERO HEATING ON VERTICAL TAIL, REYNOLDS NUMBER = 3.7 MILLION	BETA, ALPHA, ZV/BV SPDBRK	E	1-210
10	AERO HEATING ON VERTICAL TAIL, REYNOLDS NUMBER = 3.0 MILLION	BETA, ZV/BV	E	211-250
11	AERO HEATING ON VERTICAL TAIL, REYNOLDS NUMBER = 2.0 MILLION	BETA, ALPHA, ZV/BV	E	251-310
12	AERO HEATING ON VERTICAL TAIL, REYNOLDS NUMBER = 1.0 MILLION	BETA, ZV/BV	E	311-340
13	AERO HEATING ON VERTICAL TAIL, REYNOLDS NUMBER = 0.5 MILLION	BETA, ZV/BV	E	341-350
14	AERO HEATING VS BETA AT VARIOUS LOCATIONS ON VERTICAL TAIL	ALPHA, ZV/BV, XV/CV RN/L	C	351-665
	60-0 VERTICAL TAIL BETA EFFECTS (VOLUME 2 - Microfiche pages 38 through 39)			
15	BETA EFFECTS ON AERO HEATING ON THE VERTICAL TAIL	T/C NO, ALPHA, ZV/BV SPDBRK, RN/L	D	1-110
	56-0 BASIC PLOTS (VOLUME 2 - Microfiche pages 40 through 51)			
16	AERO HEATING ALONG MODEL 56-0 LEFT SIDE FUSELAGE, RN/L = 3.7 MILLION	BETA, ALPHA, ZB	F	1-65

INDEX OF DATA FIGURES (Continued)

FIGURE NUMBER	TITLE	CONDITIONS VARYING	PLOTTED COEFFICIENTS SCHEDULE	PAGES
56-0 BASIC PLOTS (continued) (VOLUME 2 - Microfiche pages 40 through 51)				
17	AERO HEATING ALONG MODEL 56-0 LEFT SIDE FUSELAGE, RN/L = 3.0 MILLION	BETA, ZB	F	66-80
18	AERO HEATING ALONG MODEL 56-0 LEFT SIDE FUSELAGE, RN/L = 2.0 MILLION	BETA, ALPHA, ZB	F	81-105
19	AERO HEATING ALONG MODEL 56-0 LEFT SIDE FUSELAGE, RN/L = 1.0 MILLION	BETA, ALPHA, ZB	F	106-120
20	AERO HEATING ALONG MODEL 56-0 LEFT SIDE FUSELAGE, RN/L = 0.5 MILLION	BETA, ALPHA, ZB	F	121-135
21	AERO HEATING VS. BETA AT VARIOUS FUSELAGE LOCATIONS (MODEL 56-0)	ALPHA, XB/LB, ZB RN/L	C	136-695
56-0 BETA EFFECTS (VOLUME 2 - Microfiche pages 52 through 54)				
22	BETA EFFECTS ON AERO HEATING (MODEL 56-0 LEFT SIDE FUSELAGE)	T/C NO, ALPHA, ZB RN/L	D	1-176
83-0 BASIC PLOTS (VOLUME 2 - Microfiche pages 55 through 59)				
23	AERO HEATING ON MODEL 83-0 CANOPY WINDOWS, RN/L = 3.7 MILLION	BETA, ALPHA, LINE	G	1-42
24	AERO HEATING ON MODEL 83-0 CANOPY WINDOWS, RN/L = 3.0 MILLION	BETA, LINE	G	43-51

INDEX OF DATA FIGURES (Continued)

FIGURE NUMBER	TITLE	CONDITIONS VARYING	PLOTTED COEFFICIENTS SCHEDULE	PAGES
83-0 BASIC PLOTS (continued) (VOLUME 2 - Microfiche pages 55 through 59)				
25	AERO HEATING ON MODEL 83-0 CANOPY WINDOWS, RN/L = 2.0 MILLION	BETA, ALPHA, LINE	G	52-69
26	AERO HEATING ON MODEL 85-0 CANOPY WINDOWS, RN/L = 1.0 MILLION	BETA, ALPHA, LINE	G	70-81
27	AERO HEATING ON MODEL 83-0 CANOPY WINDOWS, RN/L = 0.5 MILLION	BETA, ALPHA, LINE	G	82-93
28	AERO HEATING VS. BETA ON CANOPY WINDOWS, (MODEL 83-0)	RN/L, ALPHA, LINE RAY	C	94-275
83-0 BETA EFFECTS (VOLUME 2 - Microfiche pages 60 through 62)				
29	BETA EFFECTS ON AERO HEATING (MODEL 83-0 CANOPY WINDOW)	T/C NO, ALPHA, RAY RN/L	D	1-154

PLOTTED COEFFICIENT SCHEDULES:

(A): $h.9_{T_o}/h_{ref}$ vs. Z_o

(B): $h.9_{T_o}/h_{ref}$ vs. α

(C): $h.9_{T_o}/h_{ref}$ vs. β

(D): $h.9_{T_{o\beta=x}}/h.9_{T_{o\beta=o}}$ vs. $|\beta|$

(E): $h.9_{T_o}/h_{ref}$ vs. X_v/C_v

(F): $h.9_{T_o}/h_{ref}$ vs. XB/LB

(G): $h.9_{T_o}/h_{ref}$ vs. T/C NO.

*Due to the volume of plotted data, only representative plots from the first figure number in each category are presented in volume 1. Complete plotted data, on microfiche only, are published in volume 2.

INTRODUCTION

This report contains data from wind tunnel tests in the AEDC/VKF Hypersonic Tunnel B. The tests were conducted during the period from October 27 to November 24, 1980 for a total of 48.1 occupancy hours.

The objective of these tests was to obtain heating data for the orbiter in yaw.

Tests were conducted at free-stream total temperatures of 800 and 890^{o} F, simulating free air at a Mach number of 8.0 with corresponding Reynolds numbers of 0.5, 1.0, 2.0, 3.0 and 3.7x10^{6}/ft.

The model attitude varied in angle of attack from 20 to 40 degrees with yaw angles of 0, $\pm$0.5, $\pm$1 and $\pm$2 degrees.

NOMENCLATURE

Symbol	Mnemonic	Description
α	ALPHA	Angle of attack, deg
b		Model skin thickness, in. or ft. as noted
	B	Wing span, in. (see Fig. 2)
B_V	BV	Height of model vertical tail, in. (see Fig.2)
β	BETA	Sideslip angle of model (deg)
$\lvert\beta\rvert$		Absolute value of sideslip angle, deg.
c		Model material specific heat, Btu/lbm-^oR
C	C	Local chord of wing or vertical tail, in. (see Fig. 2)
δ_e	ELEVON	Elevon deflection angle, deg
δ_{SB}	SPDBRK	Speed brake deflection angle, deg
	DTW/DT	Derivative of the model wall temperature with respect to time. ^oR/sec
	HAW/HT	Recovery factor = .85, .9, 1.0
h_{ref}	HREF	Reference heat transfer coefficient (see Data Reduction)
	H(TR)	Heat transfer coefficient based on TR, QDOT/(TR-TW), Btu/ft^2-sec-^oR
	H(TT)	Heat transfer coefficient based on TT, QDOT/(TT-TW), Btu/ft^2-sec-^oR
	H(TRAX)	Heat transfer coefficient calculated using a finite element computer code (Ref. 4)
	H/HREF	Ratio of H(TT) and HREF
$h._9T_o/h_{ref}$		Ratio of H(TT) at a recovery factor of 0.9 and HREF

Symbol	Mnemonic	Description
H(0.9TT)	H(9TT)	Heat transfer coefficient based on (0.9TT), QDOT/(0.9TT-TW), Btu/ft^2-sec-^{o}R
H(0.85TT)	H85TT	Heat transfer coefficient based on (0.85TT), QDOT/(0.85TT-TW), Btu/ft^2-sec-^{o}R
	L	Reference length, in. (see Fig. 2)
	LINE	Dimension used to locate canopy thermocouples (see Table VI)
MACH,M	MACH	Free-stream Mach number
	MODEL	Orbiter model installed
	MU	Dynamic viscosity based on free-stream temperature, lbf-sec/ft^2
MUTT		Dynamic viscosity based on TT, lbf-sec/ft^2
	PO,P	Free-stream static pressure, psia
(PCK)$^{1/2}$, $\sqrt{PCK}$		Square root of the product of the model density, specific heat, and thermal conductivity; Btu/ft^2-sec$^{1/2}$ ^{o}R
P_T	PT	Tunnel stilling chamber pressure, psia
	PT2	Stagnation pressure downstream of a normal shock, psia
	PHI	Radial angle location of thermocouple in model coordinates, deg (see Figs. 2 and 7)
	PHII	Indicated roll angle, deg
	Q	Free-stream dynamic pressure, psi
	QDOT	Heat-transfer rate, Btu/ft^2-sec
	RAY	Dimension used to locate canopy thermocouples (see Table VI)

NOMENCLATURE (Continued)

Symbol	Mnemonic	Description
RE	PN/L	Free-stream unit Reynolds number, $x10^{-6}$, ft^{-1}
	RHO	Free-stream density, lbm/ft^3
RN		Reference nose radius, (0.0175 ft or 0.04 ft, determined by model scale)
RUN	RUN	Data set identification number
STN NO	STN NO	Stanton number based on reference conditions
t	t	Time from start of model injection cycle, sec
t_i	t_i	Time when initial model wall temperature was recorded before model injection, sec
	TO	Free-stream static temperature, ^oR or ^oF
T/C	T/C NO	Thermocouple identification number
TI		Initial wall temperature before injection into the flow, ^oR or ^oF
TIME		Elapsed time from lift-off, sec
TIMEEXP		Time of exposure to the tunnel flow when the data were recorded, [TIME - (0.56)(TIMEINJ)], sec
TIMEINJ		Elapsed time from lift-off to arrival at tunnel centerline, sec
TPC	TPC	Phase-change paint temperature, at which coating changes from solid to liquid, ^oR, or ^oF
TR	TR	Assumed recovery temperature, ^oR, or ^oF
	TT	Tunnel stilling chamber temperature, ^oR or ^oF
	TW	Model surface temperature, ^oR or ^oF
	V	Free-stream velocity, ft/sec
	X	Model scale longitudinal coordinate from model nose or leading edge of wing or vertical tail (see Fig. 2 and 7), in.

NOMENCLATURE (Concluded)

Symbol	Mnemonic	Description
	XO	Full scale longitudinal coordinate from a point 235 in. ahead of the orbiter nose, (see Fig. 7) in.
X_B/L_B	X/L	Thermocouple longitudinal location as a ratio of model length from model nose tip
$(X/C)_V, X_V/C_V$	XV/CV	Thermocouple location as a ratio of vertical tail chord
$(X/C)_W, X_W/C_W$	XW/CW	Thermocouple location as a ratio of wing chord
	Y	Model scale lateral coordinate (see Fig. 2), in.
	YAW	Yaw angle of model, deg
	YO	Full scale lateral coordinate, in.
2Y/B	2Y/BW	Thermocouple location as a ratio of wing semi-span
	Z	Model scale vertical coordinate (see Fig. 2), in.
Z_o, Z_B	Z_O,ZB	Full scale vertical coordinate, in. (measured from centerline of tank)
$(Z/B)_V, Z_V/B_V$	ZV/BV	Thermocouple location as a ratio of vertical tail height
β		Semi-infinite slab parameter, H(TR) $\sqrt{\text{TIMEEXP}}/\sqrt{\text{PCK}}$
ρ		Model material density, lbm/ft^3

CONFIGURATIONS INVESTIGATED

Three space shuttle orbiter models were used to obtain the thin-skin thermocouple data for this test. Two of the test articles were 0.0175-scale models of the full orbiter and were designated as the 60-0 and 56-0 models. The third model was a 0.04-scale representation of the front half of the orbiter and was identified as the 83-0 model. All of the models were supplied by Rockwell International.

The 60-0 model was a 0.0175-scale thin-skin thermocouple model of the Rockwell International Vehicle 5 configurations. The model was constructed of 17-4 PH stainless steel with a nominal skin thickness of 0.030 in. at the instrumented areas. All thermocouples were spot welded to the thin-skin inner surface.

A sketch of the 60-0 model installation in the tunnel is shown in Fig. 1. The basic dimensions and coordinate definitions for the 0.0175 scale models are shown in the sketch presented in Fig. 2. The deflection angles of the speedbrake and elevons were varied during this test and recorded on the tabulated data. The bodyflap was set at a zero deflection angle throughout the test.

The 56-0 model used for the thin-skin thermocouple portion of the test was model number 2B of the material "LH" 56-0 phase change paint model series. This was a 0.0175 scale model with the same external contour as the 60-0 model. The pilot side (left) of the fuselage has been replaced with a

thin-skin thermocouple insert contoured to the vehicle lines. This insert was constructed of 17-4 PH stainless steel with a nominal skin thickness of 0.020 in. at the thermocouple locations. A photograph of the 56-0 model injected in the tunnel is shown in Fig. 3. A sketch of the 56-0 model installation is shown in Fig. 4. The dimensions and coordinate system presented in Fig. 2 also apply to the 0.0175-scale 56-0 model.

The 83-0 model was a 0.04-scale model of the forward half of the orbiter. This model was also constructed of 17-4 PH stainless steel with a nominal skin thickness of 0.030 in. A photograph of the 83-0 model injected in the tunnel is shown in Fig. 5. The installation sketch of the 83-0 model is shown in Fig. 6 and the coordinate system and basic dimensions for the 83-0 model are presented in Fig. 7.

The model used for the phase change paint entry was from the 56-0 series constructed without the thin-skin thermocouple insert. Two 0.0175-scale removable vertical tails with the SILTS pod were fabricated of Novamide 700-55. A photograph of this model injected in the tunnel is shown in Fig. 3.

Nomenclature to describe the various components of the three models used for these tests are:

MODEL 56-0 Orbiter (Vehicle 5 configuration, VL70-000140C lines)

Component	Definition
B 62	fuselage
C 12	canopy
E 52	elevon
F 10	bodyflap
M 16	OMS pods
V 30	vertical
W 127	wing

MODEL 60-0 Orbiter (Vehicle 5 configuration, VL70-000140C lines)

Component	Definition
B 62	fuselage
C 12	canopy
E 52	elevon (δ_e = 0^o and 5^o)
F 10	bodyflap
M 16	OMS pods
R 18	rudder
V 8	vertical tail
W 116	wing
δ_{SB}	speed brakes (0 and 49 degrees)

MODEL 83-0 Orbiter (Vehicle 5 configuration, VL70-000140C lines)

Component	Definition
B 60	fuselage
C 10	canopy

Full scale and model scale dimensional data for the various components of the three models can be found in Table III.

Further model description, including some model drawings, can be found in Reference 8.

TEST INSTRUMENTATION

The 60-0 model was instrumented with 600 thirty-gauge iron-constantan and chromel-constantan thermocouples. Only 230 of these thermocouples were used on this test. Thermocouple locations for this model are illustrated in Fig. 8; the dimensional locations and skin thicknesses for the thermocouples connected on this test are listed in Table IV. The thermocouples identified by a number only are iron-constantan. The thermocouples identified by a number followed by the letter A or C are chromel-constantan that were added to the model*. The letter D after a thermocouple number designates an iron-constantan thermocouple in a new location on the OMS pod.

The 56-0 model instrumentation consisted of 80 thirty-gauge chromel-constantan thermocouples located on the thin-skin insert. All of these thermocouples were connected on this test. The thermocouple locations for this model are illustrated in Fig. 9. The dimensional locations and skin thicknesses are listed in Table V.

For this test only 94 of the 482 thirty-gauge chromel-constantan thermocouples on the 83-0 model were connected. The thermocouple locations for this model are illustrated in Fig. 10. The dimensional locations and skin thicknesses for the thermocouples used on this test are included in Table VI.

The thermocouple data were recorded on a new multiplexing system that is capable of recording a maximum of 256 thermocouple channels during each run.

*Note: In the tabulated data, thermocouple numbers ending in A or C appear instead as 2000 or 1000 series numbers, respectively.

This increased capacity greatly increases efficiency by reducing the need for multiple runs. The maximum number of thermocouples recorded during one run was 230 when the 60-0 model was installed. All 80 thermocouples were connected on the 56-0 model and 94 were connected on the 83-0 model. Some of the listed thermocouples were determined to be inoperative during the test and these have been deleted from the tabulated data. (See Table VIII)

The phase-change paint technique of obtaining heat-transfer data uses a fusible coating which changes from an opaque solid to a transparent liquid (i.e., it melts) at a specified temperature (TPC). The demarcations between melted and unmelted paint (melt lines) are model surface isotherms and are used to compute the aerodynamic heating. Tempilaq paint was used as the phase-change coating for these tests. The calibrated melting points of the paints used were 250, 300, 350, 450, 550, 600 and 700^{o}F. A more complete description of the phase-change paint technique is presented in Ref. 2.

TEST FACILITY DESCRIPTION

The Arnold Engineering Development Center (AEDC) is an Air Force Facility located in Tullahoma, Tennessee. The tunnel used, Tunnel B, is located in the Von Karman Facility (VKF) portion of this center. Engineering and other technical operations in this tunnel are performed by contractor personnel of ARO, Inc.

Tunnel B (Fig. 11) is a continuous, closed circuit, variable density wind tunnel with an axisymmetric contoured nozzle and a 50-inch diameter test section. The tunnel can be operated at a nominal Mach number of 6 or 8 at stagnation pressures from 20 to 300 and 50 to 900 psia, respectively, and at a stagnation temperature of up to 1350°R. The model may be injected into the tunnel for a test run and then retracted for model cooling or model changes without interrupting the tunnel flow.

TEST PROCEDURE

In the VKF continuous flow wind tunnels (A, B, C), the model is mounted on a sting support mechanism in an installation tank directly underneath the tunnel test section. The tank is separated from the tunnel by a pair of fairing doors and a safety door. When closed, the fairing doors, except for a slot for the pitch sector, cover the opening to the tank and the safety door seals the tunnel from the tank area. After the model is prepared for a data run, the personnel access door to the installation tank is closed, the tank is vented to the tunnel flow, the safety and fairing doors are opened, and the model is injected into the airstream. After the data are obtained, the model is retracted into the tank and the sequence is reversed with the tank being vented to atmosphere to allow access to the model in preparation for the next run. A given injection cycle is termed a run, and all the data obtained are identified in the data tabulations by a run number.

Prior to each test run, the model temperatures were monitored to ensure that they were nominally $70^{\circ}F$. The model was then injected at the desired test attitude as the data acquisition sequence commenced.

The model remained on the tunnel centerline for about three seconds and was then retracted into the installation tank. The model was then cooled and repositioned for the next injection.

A 256 channel multiplexing analog-to-digital converter was used in conjunction with a Digital Equipment Corporation (DEC) PDP-11 computer and a DEC-10 computer to record the temperature data. The system sampled the output of each thermocouple approximately 17 times per second.

For phase-change paint tests the model was painted with the appropriate Tempilaq paint, and the model surface initial temperature (TI) was measured with a thermocouple probe. The model was positioned to the test attitude and injected into the tunnel flow for about 10 sec. During this time three 70-mm sequence cameras using color film photographed the progression of the paint melt lines. These cameras were triggered simultaneously at a nominal rate of two frames/sec while an analog-to-digital scanner recorded the precise timing. After the model was retracted from the tunnel flow, it was cooled and cleaned with an alcohol bath before being repainted for the next test run. For this test only the vertical tail and the SILTS pod were painted with phase-change paint.

Instrumentation outputs were recorded using the VKF data acquisition system under the control of a PDP 11/40 computer. The triggering of the cameras and the frame rate was controlled by a separate control system.

Preparation of the model for an oil-flow run was the same as for the phase-change paint runs except that oil was applied to the model in place of the paint. Four sequence cameras were used to photograph the oil-flow patterns.

DATA REDUCTION

Thin-Skin Thermocouple Data

The reduction of thin-skin temperature data to coefficient form normally involves only the calorimeter heat balance for the thin-skin as follows:

$$QDOT = \rho bc\ DTW/DT \tag{1}$$

$$H(TR) = \frac{QDOT}{TR-TW} = \frac{\rho bc\ DTW/DT}{TR-TW} \tag{2}$$

Thermal radiation and heat conduction effects on the thin-skin element are neglected in the above relationship and the skin temperature response is assumed to be due to convective heating only. It can be shown that for constant TR, the following relationship is true:

$$\frac{d}{dt}\left(\ln\left[\frac{TR-TI}{TR-TW}\right]\right) = \frac{DTW/DT}{TR-TW} \tag{3}$$

Substituting Eq. (3) in Eq. (2) and rearranging terms yields:

$$\frac{H(TR)}{\rho bc} = \frac{d}{dt}\left(\ln\left[\frac{TR-TI}{TR-TW}\right]\right) \tag{4}$$

By assuming that the value of $H(TR)/\rho bc$ is a constant, it can be seen that the derivative (or slope) must also be constant. Hence, the term

$$\ln\left[\frac{TR-TI}{TR-TW}\right]$$

is linear with time. This linearity assumes the validity of Eq. (2) which applies for convective heating only. The evaluation of conduction effects will be discussed later.

The assumption that H(TR) and c are constant is reasonable for this test although small variations do occur in these parameters. The variations of H(TR) caused by changing wall temperature and by transition movement with wall temperature are trivial for the small wall temperature changes that occur during data reduction. The value of the model material specific heat, c, was computed by the relation

$$c = 0.0797 + (5.556 \times 10^{-5})TW, \text{ (17-4 PH stainless steel)} \qquad (5)$$

The maximum variation of c over any curve fit was less than 1.5 percent. Thus, the assumption of constant c used to derive Equation 4 was reasonable. The value of density used for the 17-4 PH stainless steel skin was, $\rho = 490$ lbm/ft^3, and the skin thickness, b, for each thermocouple is listed in Tables IV, V and VI.

The right side of Equation 4 was evaluated using a linear least squares curve fit of 15 consecutive data points to determine the slope. The start of the curve fit coincided with the model arrival on the tunnel centerline. For each thermocouple the tabulated value of H(TR) was calculated from the slope and the appropriate values of ρbc; i.e.,

$$H(TR) = \rho bc \frac{d}{dt}\left(\ln\left[\frac{TR-TI}{TR-TW}\right]\right) \qquad (6)$$

To investigate conduction effects, a second value of H(TR) was calculated at a time one second later. A comparison of these two values was used to identify those thermocouples that were influenced by significant conduction

(or system noise). The data for a given thermocouple were deleted if the values of H(TR) differed by more than 35 percent. In general, conduction and/or noise effects were found to be negligible.

Since the value of TR is not known at each thermocouple location it has become standard procedure to use three assumed values of TR. The assumed values are 1.0TT, 0.9TT and 0.85TT. The use of these assumed values of TR provides an indication of the sensitivity of the heat-transfer coefficients to the value of TR assumed. As can be noted in the tabulated data, there are large percentage differences in the values of the heat-transfer coefficients calculated from the three assumed values. Therefore, if the data are to be used for flight predictions, the value selected for TR is obviously very important and is a function of model location and boundary layer state.

The heat-transfer coefficient calculated from Eq. 4 was normalized using the Fay-Riddell stagnation point coefficient, H(REF), based on a nose radius of 1.0 ft full scale. The reference nose radius, RN, used to calculate HREF is either 0.0175 ft or 0.04 ft as determined by the model scale.

For phase-change paint tests, the data were reduced by assuming that the model wall heating can be represented by a thermally semi-infinite slab. A material with a low thermal diffusivity is necessary for this assumption

to be valid for reasonable model wall thicknesses (>0.25 in.) consistent with the Tunnel B data acquisition times of 3 to 30 sec.

Data reduction of the melt line photographs was accomplished by identifying these isothermal lines for various times during the test run. These isothermal lines are related to corresponding aerodynamic heat-transfer coefficients, H(TR), by applying the semi-infinite slab heat equation, given below.

$$\frac{TPC-TI}{TR-TI} = 1 - e^{\beta^2} \operatorname{erfc} \beta \tag{7}$$

where

$$\beta = \frac{H(TR)\sqrt{TIMEEXP}}{\sqrt{PCK}} \text{ , erfc = error function} \tag{8}$$

and

TIMEEXP = time of heating

The lumped material thermophysical property $\sqrt{PCK}$ for the Novamide 700-55 material was provided by Rockwell. The value of $\sqrt{PCK}$ was a function of temperature and the values used are listed in Table IX. The heat-transfer coefficients were computed for assumed adiabatic recovery temperatures TT, 0.9TT, and 0.85 TT except when the paint temperature was 700°F. In this case only TT was used because of the small difference between TT and TPC. The Fay-Riddell stagnation point heat-transfer coefficient, based on a 0.0175-ft-radius sphere, was used to normalize the computed aerodynamic

heat-transfer coefficient. (The radius of this hypothetical sphere would be 1 ft at corresponding orbiter full-scale conditions).

The tabulated data are based on the assumption of a semi-infinite slab. In the case of the SILTS pod with a small radius (0.187 in.) the actual heat transfer coefficient values will deviate from those calculated based on the semi-infinite slab assumption. A finite element computer program, Ref. 4, was used to model the SILTS pod geometry and to compute the heat-transfer coefficient at the stagnation point. The heat-transfer coefficient determined from the semi-infinite slab assumption, H(TT), is ratioed to the computed value H(TRAX) for the stagnation point in Fig. 12. The application of this "correction factor" to the data is illustrated in the following example. Consider a case where the tabulated data (based on semi-infinite slab) was obtained at 5 sec and the level of the heat transfer coefficient was 0.02. From Fig. 12 this gives a value of H(TT)/H(TRAX) = 1.3. Thus to adjust (ADJ) the semi-infinite slab tabulated data to that of an axisymmetric element on the hemispherical nose cap we have

$$H(TT)_{ADJ} = \left[H(TT)_{TAB\ DATA}\right]\left[\frac{1}{\frac{H(TT)}{H(TRAX)}}\right] \tag{9}$$

$$= 0.02\ \frac{1}{1.3}$$

$$= 0.0154 \text{ i.e.} \simeq 23\% \text{ lower than tabulated data.}$$

It is important to emphasize that the intent of Fig. 12 is only to provide an estimate of the approximate magnitude of the 3-D effects and it is not intended that all the data be "corrected" for 3-D effects.

Reference Heat-Transfer Coefficients

In presenting heat-transfer coefficient results it is convenient to use reference coefficients to normalize the data. Equilibrium stagnation point values derived from the work of Fay and Riddell (Ref. 10) were used to normalize the data obtained in this test. These reference coefficients are given by:

$$H(REF) = \frac{8.17173(PT2)^{1/2}(MUTT)^{0.4}\left[1-\frac{P}{PT2}\right]^{0.25}\left[0.2235+(1.35\times10^{5})(TT+560)\right]}{(RN)^{1/2}(TT)^{0.15}}$$

and

$$STFR = \frac{H(REF)}{(RHO)(V)\left[0.2235+(1.35\times10^{-5})(TT+560)\right]}$$

where

PT2	Stagnation pressure downstream of a normal shock wave, psia
MUTT	Air viscosity based on TT, lb_f-sec/ft^2
P	Free-stream pressure, psia
TT	Tunnel stilling chamber temperature, ^oR
RN	Reference nose radius, (0.0175 ft or 0.04 ft determined by model scale)

REFERENCES

1. Test Facilities Handbook (Eleventh Edition). "von Karman Gas Dynamics Facility, Vol. 3." Arnold Engineering Development Center, June 1979.

2. Jones, Robert A. and Hunt, James L., "Use of Fusible Temperature Indicators for Obtaining Quantitative Aerodynamic Heat-Transfer Data", NASA-TR-R-230, February 1966.

3. Thompson, J. W. and Abernethy, R. B. et al. "Handbook Uncertainty in Gas Turbine Measurements", AEDC-TR-73-5 (AD755356), February 1973.

4. Rochell, J. K., "TRAX - A Finite Element Computer Program for Transient Heat Conduction Analysis of Axisymmetric Bodies", University of Tennessee Space Institute Master's Thesis, June 1973.

5. Nossaman, G. O., "Feasibility Study for Automatic Reduction of Phase Change Imagery", NASA CR-112001, 1971.

6. MCR-7172, Wind Tunnel Tests to Obtain Heating Data for Orbiter in Yaw.

7. Dr. Serge-Albert Waiter, "Determination of Temperature Efficiency $R = T_{aw}/T_o$ in Low Temperature Wind Tunnels (An Engineering Attempt)", NA-77-299, Prepared for the 47th Semi-annual Meeting of the Supersonic Tunnel Association, April 1977.

8. SOD-80-0303, "Pretest Information for Testing the 56-Ø, 60-Ø (0.0175 Scale) and 83-Ø (0.04-scale) Thin Skin Thermocouple Insert Models in the AEDC/VKF-B Wind Tunnel (Test OH-109)".

9. AEDC-TSR-81-V6, "Test Results from the NASA/Rockwell International Space Shuttle Orbiter in Yaw Heating Test (OH-109)."

10. Fay, J. A. and Riddell, F. R., "Theory of Stagnation Point Heat Transfer in Dissociated Air", Journal of the Aeronautical Sciences, Vol. 25, No. 2, February 1958.

TABLE I. TEST CONDITIONS

The test was conducted at a nominal Mach number of 8 in Tunnel B. A summary of the specific test conditions is given below.

MACH NO.	PT, psia	TT, ^{o}R	Q, psia	P, psia	RE x 10^{-6}, ft^{-1}
7.83	100	1250	0.5	0.010	0.5
7.84	120	1245	0.6	0.014	0.6
7.88	205	1260	1.0	0.020	1.0
7.93	435	1300	2.0	0.050	2.0
7.96	670	1320	3.1	0.070	3.0
7.97	850	1350	3.9	0.090	3.7

A more detailed test summary showing all configurations tested and the variables for each is presented in Table II.

TABLE II

TEST : ϕH109 (AEDC V41B-G9) — DATA SET/RUN NUMBER COLLATION SUMMARY — DATE : 11/6/80

DATA SET IDENTIFIER	CONFIGURATION	α	δ_e	δ_{SB}	RN/L	P_T	M	SIDESLIP ANGLE ~ β (deg) -2.0	-1.0	-0.5	0.0	0.5	1.0	2.0	TEST RUN NUMBERS
R4Z*01	MODEL 60-ϕ	20	0	49	3.7	850	8.0	14	12	10	1	4	6	8	
02		20									2				
03		20									17				
04		25						15	13	11	3	5	7	9	
05		25		↓					16						
06		20		0				94	48	42	18	24	30	36	
07		20									54				
08		25						95	49	43	19	25	31	37	
09		27.5						96	50	44	20	26	32	38	
10		30						97	51	45	21	27	33	39	
11		32.5						98	52	46	22	28	34	40	
12		35			↓	↓		99	53	47	23	29	35	41	
13		35			3.0	670		85	86	87		90	89	88	
14		35			↓	↓		92							
15		35			2.0	435		75	74	73	69	70	71	72	
16		35									84				
17		40						76	77	78	83	82	81	79	
18		40	↓	↓	↓	↓	↓							80	

* B - FUSELAGE
ϕ - OMS POD
U - UPPER WING
V - VERTICAL TAIL

α OR β SCHEDULES

NASA-MSFC-MAF

TABLE II (Continued)

TEST : ΦH109 (AEDC V41B-G9) — DATA SET/RUN NUMBER COLLATION SUMMARY — DATE : 11/6/80

DATA SET IDENTIFIER	CONFIGURATION	α	δe	δSB	R/L	PT	M	SIDESLIP ANGLE ~ β (deg) -2.0	-1.0	-0.5	0.0	0.5	1.0	2.0	TEST RUN NUMBERS
R4Z*19	MODEL 60-Φ	40	0	0	1.0	205	8.0	55	56	57	61	60	59	58	
20		40									62				
21		40			0.5	100				66	63	64			
					-OIL FLOW RUNS-										
		20	0	0	3.7	850	8.0				105 205				
		25									104 206				
		27.5									103 209				
		30									102 207				
		35									101 208				
		40			2.0	435					106				
		40			1.0	205					107				
		40			0.5	100					108				
		30	5	0	3.7	850					200				
		35									201				
		40			2.0	435					202				
		40			1.0	205					203				
		40			0.5	100					204				

* B - FUSELAGE
Φ - OMS POD

α OR β SCHEDULES
U - UPPER WING
V - VERTICAL TAIL

NASA-MSFC-MAF

TABLE II (Continued)

TEST: ΦH109 (AEDC V41B-G9) — DATA SET/RUN NUMBER COLLATION SUMMARY — DATE: 11/6/80

DATA SET IDENTIFIER	CONFIGURATION	α	δe	δSB	RN/L	PT	M	SIDESLIP ANGLE ~ β (deg) -2.0	-1.0	-0.5	0.0	0.5	1.0	2.0	TEST RUN NUMBERS
R4Z★23	MODEL 83-O	20	—	—	3.7	850	8.0	180	178	167	143	154	155	166	
24		20									186				
25		25						181	177	168	144	153	156	179	
26		27.5						182	176	169	145	152	157		
27		30						183	175	170	146	151	158	163	
28		32.5						184	174	171	147	150		162	
29		35						185	173	172	148	149	160	161	
30		35			↓	↓		165							
31		35			3.0	670		187	188	189	193	192	191	190	
32		35			↓	↓		194							
33		20			2.0	435					124				
34		35						115	114	113	109	110	111	112	
35		35									123				
36		40			↓	↓		116	117	118	122	121	120	119	
37		20			1.0	205					125				
38		40						132	131	130	126	127	128	129	
39		40			↓	↓					133				
40		20			0.5	100					141				
41		40						140	138	136	134	135	137	139	
↓ 42	↓	40	↓	↓	↓	↓	↓				142				

OIL FLOW: RN/FT = 3.7, β = 0°, α = 30, 35, 40

Run Number = 195, 196, 197, 198, 199

★ B - FUSELAGE
C - CANOPY

α OR β SCHEDULES

NASA-MSFC-MAF

TABLE II (Concluded)

TEST : ØH109 (AEDC V41B-G9) — DATA SET/RUN NUMBER COLLATION SUMMARY — DATE : 11/6/80

DATA SET IDENTIFIER	CONFIGURATION	α	δe	δSB	RN/ft	PT	M	SIDESLIP ANGLE ~ β (deg) -2.0	-1.0	-0.5	0.0	0.5	1.0	2.0	TEST RUN NUMBERS
R4ZB43	MODEL 56-Ø	20	0	0	3.7	850	8.0	246	245	234	210	221	222	233	
44		20									252				
45		25						247	244	235	211	220	223	232	
46		27.5						248	243	236	212	219	224	231	
47		30						249	242	237	213	218	225	230	
48		32.5						250	241	238	214	217	226	229	
49		35			↓	↓		251	240	239	215	216	227	228	
50		35			3.0	670		253	254	255	259	258	257	256	
51		35			↓	↓		260							
52		35			2.0	435		267	266	265	261	262	263	264	
53		35			↓	↓					275				
54		40			↓	↓		268	269	270	274	273	272	271	
55		40			1.0	205		282	281	280	276	277	278	279	
56		40			↓	↓					283				
57		40			0.5	100		290	288	286	284	285	287	289	
58		40			↓	↓					291				
R4Z*59	MODEL 60-Ø	20			3.7	850					100				
60		35	↓	↓	3.0	670	↓	93							

α OR β SCHEDULES: NO OIL FLOW TESTS ON MODEL 56-Ø

NASA-MSFC-MAF

TABLE III MODEL DIMENSIONAL DATA

MODEL DIMENSIONAL DATA

MODEL COMPONENT : BODY - B_{60}

GENERAL DESCRIPTION : 50% orbiter forebody, vehicle 140C.

NOTE: This body includes a small portion of the wing glove.

MODEL SCALE: 0.040 (83-0 MODEL)

DRAWING NUMBER : VL70-000140C

DIMENSIONS :	FULL SCALE	MODEL SCALE
Length	645.15	25.80
Max Width	330.00	13.20
Max Depth		
Fineness Ratio		
Area		
Max. Cross-Sectional		
Planform		
Wetted		
Base		

TABLE III. (Continued)
MODEL DIMENSIONAL DATA

MODEL COMPONENT : BODY - B_{62}

GENERAL DESCRIPTION : Configuration 140C orbiter fuselage, MCR 200-R4. Similar to 140A/B fuselage except aft body revised and improved midbody-wing-boot fairing, X_o = 940 to X_o = 1040.

MODEL SCALE: 0.0175 (56-0 & 60-0 MODELS)

DRAWING NUMBER : VL70-000140C, -000202C, -000205A
VL70-000200B, -000203

DIMENSIONS :	FULL SCALE	MODEL SCALE
Length (IML: FWD Sta X_o=238), In.	1290.3	22.58
Length (OML: Fwd Sta X_o=235), In.	1293.3	22.63
Max Width (At X_o = 1528.3), In.	264.0	4.62
Max Depth (At X_o = 1464), In.	250.0	4.38
Fineness Ratio	4.899	4.899
Area - Ft^2		
Max. Cross-Sectional	340.885	0.104
Planform		
Wetted		
Base		

TABLE III (Continued)

MODEL DIMENSIONAL DATA

MODEL COMPONENT : CANOPY - C_{10}

GENERAL DESCRIPTION : Configuration 4 canopy and windshield as used with B_{25}, six glass panes in windshield.

MODEL SCALE: 0.040, (83-0 MODEL)

DRAWING NUMBER : VL70-000140B, 140C, 202B

DIMENSIONS :	FULL SCALE	MODEL SCALE
Length (X_o =434.643 to 670), In.	235.357	9.414
Max Width		
Max Depth (Glass, In.	28.00	1.12
Fineness Ratio		
Area		
Max. Cross-Sectional		
Planform		
Wetted		
Base		
Nose/windshield intersection, X_o =	434.643	17.386

TABLE III. (Continued)
MODEL DIMENSIONAL DATA

MODEL COMPONENT : CANOPY - C_{12}

GENERAL DESCRIPTION : Configuration 140C orbiter canopy. Vehicle cabin No. 31 updated to MCR 200-R4. Used with fuselage B_{62}.

MODEL SCALE: 0.0175 (56-0 & 60-0 MODELS)

DRAWING NUMBER : VL70-000140C, -000202B, -000204

DIMENSIONS :	FULL SCALE	MODEL SCALE
Length (X_o = 434.643 to 578), In.	143.357	2.508
Max Width (At X_o = 513.127), In.	152.412	2.667
Max Depth (Z_o = 501 to 449.39), In.	51.61	0.903
Fineness Ratio		
Area		
Max. Cross-Sectional		
Planform		
Wetted		
Base		

TABLE III. (Continued)
MODEL DIMENSIONAL DATA

MODEL COMPONENT: ELEVON - E_{52}

GENERAL DESCRIPTION: Elevon for configuration 140C. Hingeline at X_o = 1387, elevon split line Y_o = 312.5, 6.0", beveled edges, and centerbodies.

MODEL SCALE: 0.0175, (56-0 & 60-0 MODELS)

DRAWING NUMBER: VL70-000140C, -006089, -006092

DIMENSIONS:	FULL-SCALE	MODEL SCALE
Area - Ft^2	210.0	0.064
Span (equivalent) - In.	349.2	6.111
Inb'd equivalent chord- In.	118.0	2.065
Outb'd equivalent chord	55.19	0.966
Ratio movable surface chord/ total surface chord		
At Inb'd equiv. chord	0.2096	0.2096
At Outb'd equiv. chord	0.4004	0.4004
Sweep Back Angles, degrees		
Leading Edge	0.0	0.0
Tailing Edge	- 10.056	- 10.056
Hingeline	0.0	0.0
Area Moment (Product of area & $\bar{c}$) Ft^3	1587.25	0.008
Mean Aerodynamic Chord, In.	90.7	1.587
Hingeline dihedral (origin at Z_o = 261.3509), deg.	5.229	5.229

TABLE III(Continued)

MODEL DIMENSIONAL DATA

MODEL COMPONENT : BODY FLAP - F_{10}

GENERAL DESCRIPTION : Configuration 140C body flap. Hingeline located at X_o = 1532, Z_o = 287.

MODEL SCALE: 0.0175, (56-0 & 60-0 MODELS)

DRAWING NUMBER : VL70-000140C, -355114

DIMENSIONS :	FULL SCALE	MODEL SCALE
Length (X_o = 1525.5 to X_o = 1613), In.	87.50	1.531
Max Width (At L.E., X_o = 1525.5), In.	256.00	4.480
Max Depth (X_o = 1532), In.	19.798	0.346
Fineness Ratio		
Area - Ft^2		
Max. Cross-Sectional (At H.L.)	35.196	0.011
Planform	135.00	0.041
Wetted		
Base (X_o = 1613)	4.89	0.0015

TABLE III (Continued)

MODEL DIMENSIONAL DATA

MODEL COMPONENT : OMS POD - M_{16}

GENERAL DESCRIPTION : Configuration 140C orbiter OMS Pod - short pod.

MODEL SCALE: 0.0175 , (56-O & 60-O MODEL)

DRAWING NUMBER : VL70-008401, -008410

DIMENSIONS :	FULL SCALE	MODEL SCALE
Length (OMS Fwd Sta X_o = 1310.5), In.	258.50	4.524
Max Width (At X_o = 1511), In.	136.8	2.394
Max Depth (At X_o = 1511), In.	74.70	1.307
Fineness Ratio	2.484	2.484
Area = Ft^2		
Max. Cross-Sectional	58.864	0.018
Planform		
Wetted		
Base		

TABLE III. (Continued)

MODEL DIMENSIONAL DATA

MODEL COMPONENT: RUDDER - R_{18}

GENERAL DESCRIPTION: The rudder is a secondary movable airfoil at the trailing edge of the vertical fin that imparts yaw forces. This dimensional data was calculated from the OML master dimensions.

MODEL SCALE: 0.0175 ,(60-0 MODEL)

DRAWING NUMBER: Vehicle 5 Configuration MCR 200, Rev. 7

DIMENSIONS:	FULL-SCALE	MODEL SCALE
Area - Ft^2	97.84	0.030
Span (equivalent) - In.	198.614	3.476
Inb'd equivalent chord - In.	97.07	1.699
Outb'd equivalent chord - In.	50.80	0.889
Ratio movable surface chord/ total surface chord		
At Inb'd equiv. chord	0.400	0.400
At Outb'd equiv. chord	0.400	0.400
Sweep Back Angles, degrees		
Leading Edge	34.833	34.833
Tailing Edge	26.249	26.249
Hingeline	34.833	34.833
Area Moment (Product of Area & $\bar{c}$), Ft^3	593.889	.0032
Mean Aerodynamic Chord, In.	72.840	1.275

TABLE III. (Continued)

MODEL DIMENSIONAL DATA

MODEL COMPONENT: VERTICAL - V_8

GENERAL DESCRIPTION: Configuration 140C orbiter vertical tail (identical to configuration 140A/B vertical tail).

MODEL SCALE: 0.0175 (60-0 MODEL)

DRAWING NUMBER: VL70-000140C, -000146B

DIMENSIONS:	FULL SCALE	MODEL SCALE
TOTAL DATA		
Area (Theo) - Ft^2		
Planform	413.253	0.127
Span (Theo) - In.	315.72	5.530
Aspect Ratio	1.675	1.675
Rate of Taper	0.507	0.507
Taper Ratio	0.404	0.404
Sweep-Back Angles, Degrees.		
Leading Edge	45.000	45.000
Trailing Edge	26.25	26.25
0.25 Element Line	41.13	41.13
Chords:		
Root (Theo) WP	268.50	4.699
Tip (Theo) WP	108.47	1.898
MAC	199.81	3.497
Fus. Sta. of .25 MAC	1463.35	25.609
W.P. of .25 MAC	635.52	11.122
B.L. of .25 MAC	0.0	0.0
Airfoil Section		
Leading Wedge Angle - Deg.	10.00	10.00
Trailing Wedge Angle - Deg.	14.92	14.92
Leading Edge Radius	2.00	2.00
Void Area	13.17	0.0040
Blanketed Area	0.0	0.0

TABLE III (Continued)

MODEL DIMENSIONAL DATA

MODEL COMPONENT: VERTICAL - V_{30}

GENERAL DESCRIPTION: Slab sided vertical tail with extended span

MODEL SCALE: 0.0175, (56-O MODEL)

DIMENSIONS:	FULL SCALE	MODEL SCALE
TOTAL DATA		
Area (Theo) - Ft^2 Planform	442.299	0.135
Span - In.	358.57	6.275
Aspect Ratio	2.019	2.019
Rate of Taper	0.507	0.507
Taper Ratio	0.323	0.323
Sweep-Back Angles, Degrees		
Leading Edge	45.000	45.000
Trailing Edge	26.25	26.25
0.25 Element Line	41.13	41.13
Chords:		
Root (Theo) WP	268.50	4.699
Tip (Theo) WP	86.75	1.518
MAC	193.12	3.380
Fus. Sta. of .25 MAC	1474.87	25.810
W.P. of .25 MAC	648.71	11.352
B.L. of .25 MAC	0.0	0.0
Airfoil Section		
Leading Wedge Angle - Deg.	11.75	11.75
Trailing Wedge Angle - Deg	0.0	0.0
Leading Edge Radius	0.0	0.0
Void Area	0.0	0.0
Blanketed Area	0.0	0.0

TABLE III. (Continued)

MODEL DIMENSIONAL DATA

MODEL COMPONENT: WING-W_{116}

GENERAL DESCRIPTION: Configuration 5

NOTE: Identical to W_{114} except airfoil thickness. Dihedral angle is along trailing edge of wing. Geometric twist = 0.

MODEL SCALE: 0.0175 , (60-0 MODEL)

TEST NO.

DWG. NO. VL70-000140A, -000200

DIMENSIONS:	FULL-SCALE	MODEL SCALE
TOTAL DATA		
Area (Theo.) Ft^2 Planform	2690.0	0.824
Span (Theo.) In.	936.68	16.392
Aspect Ratio	2.265	2.265
Rate of Taper	1.177	1.177
Taper Ratio	0.200	0.200
Dihedral Angle, degrees	3.500	3.500
Incidence Angle, degrees	0.500	0.500
Aerodynamic Twist, degrees		
Sweep Back Angles, degrees		
Leading Edge	45.000	45.000
Trailing Edge	- 10.056	- 10.056
0.25 Element Line	35.209	35.209
Chords:		
Root (Theo) B.P.0.0.	689.24	12.062
Tip, (Theo) B.P.	137.85	2.412
MAC	474.81	8.309
Fus. Sta. of .25 MAC	1136.83	19.895
W.P. of .25 MAC	290.58	5.085
B.L. of .25 MAC	182.13	3.187
EXPOSED DATA		
Area (Theo) Ft^2	1751.50	0.536
Span, (Theo) In. BP108	720.68	12.612
Aspect Ratio	2.059	2.059
Taper Ratio	0.245	0.245
Chords		
Root BP108	562.09	9.837
Tip 1.00 $\frac{b}{2}$	137.85	2.412
MAC	392.83	6.875
Fus. Sta. of .25 MAC	1185.98	20.755
W.P. of .25 MAC	294.30	5.150
B.L. of .25 MAC	251.77	4.406
Airfoil Section (Rockwell Mod NASA) XXXX-64		
Root $\frac{b}{2}$ =	0.113	0.113
Tip $\frac{b}{2}$ =	0.120	0.120
Data for (1) of (2) Sides		
Leading Edge Cuff Planform Area Ft^2	119.18	0.035
Leading Edge Intersects Fus M. L. @ Sta	500.00	8.750
Leading Edge Intersects Wing @ Sta	1024.00	17.920

TABLE III (Concluded)
MODEL DIMENSIONAL DATA

MODEL COMPONENT: WING-W_{127}

GENERAL DESCRIPTION: Configuration 140C orbiter wing, MCR 200-R4. Similar to 140A/B wing W_{116} but with refinements: improved wing-boot-midbody fairing (X_o = 940 to X_o = 1040). Elevon split line relocated from Y_o = 281 to Y_o = 312.5).

MODEL SCALE: 0.0175, (56-0 MODEL)

TEST NO. DWG. NO. VL70-000140C, -000200B

DIMENSIONS:	FULL-SCALE	MODEL SCALE
TOTAL DATA		
Area (Theo.) Ft^2 Planform	2690.00	0.824
Span (Theo In.	936.68	16.392
Aspect Ratio	2.265	2.265
Rate of Taper	1.177	1.177
Taper Ratio	0.200	0.200
Dihedral Angle, degrees	3.500	3.500
Incidence Angle, degrees	0.500	0.500
Aerodynamic Twist, degrees	3.000	3.000
Sweep Back Angles, degrees		
Leading Edge	45.000	45.000
Trailing Edge	- 10.065	- 10.065
0.25 Element Line	35.209	35.209
Chords:		
Root (Theo) B.P.0.0.	689.24	12.062
Tip, (Theo) B.P.	137.85	2.412
MAC	474.81	8.309
Fus. Sta. of .25 MAC	1136.83	19.895
W.P. of .25 MAC	290.58	5.085
B.L. of .25 MAC	182.18	3.187
EXPOSED DATA		
Area (Theo) Ft^2	1751.50	0.536
Span, (Theo) In. BP108	720.68	12.612
Aspect Ratio	2.059	2.059
Taper Ratio	0.245	0.245
Chords		
Root BP108	562.09	9.837
Tip 1.00 $\frac{b}{2}$	137.85	2.412
MAC	392.83	6.875
Fus. Sta. of .25 MAC	1185.98	20.755
W.P. of .25 MAC	294.30	5.150
B.L. of .25 MAC	251.77	4.406
Airfoil Section (Rockwell Mod NASA) XXXX-64		
Root $\frac{b}{2}$ =	0.113	0.113
Tip $\frac{b}{2}$ =	0.120	0.120
Data for (1) of (2) Sides		
Leading Edge Cuff Planform Area Ft^2	113.18	0.035
Leading Edge Intersects Fus M. L. @ Sta	500.00	8.750
Leading Edge Intersects Wing @ Sta	1024.0	17.920

TABLE IV. 60-0 Model Thermocouple Locations

Vertical Tail			
T/C	$(X/C)_V$	$(Z/B)_V$	b, in.
340	0.1	0.1	0.0315
341	0.3	0.1	0.0305
344	0.2	0.2	0.0302
345	0.4	0.2	0.0313
347	0.8	0.2	0.0315
349	0.2	0.3	0.0310
350	0.4	0.3	0.0310
351	0.5	0.3	0.0318
352	0.9	0.3	0.030
354	0.2	0.4	0.0315
356	0.5	0.4	0.0306
357	0.7	0.4	0.0290
358	0.9	0.4	0.0298
361	0.9	0.5	0.0315
363	0.1	0.6	0.0295
364	0.2	0.6	0.0303
365	0.4	0.6	0.0318
366	0.5	0.6	0.0315
367	0.7	0.6	0.0280
368	0.9	0.6	0.030
370	0.7	0.7	0.0275
371	0.9	0.7	0 0290
373	0.1	0.8	0.0293
374	0.4	0.8	0.0310
375	0.5	0.8	0.0325

Vertical Tail			
T/C	$(X/C)_V$	$(Z/B)_V$	b, in.
376	0.7	0.8	0.0280
377	0.9	0.8	0.0290
378	0.1	0.9	0.0310
379	0.3	0.9	0.0305
380	0.5	0.9	0.0320
381	0.7	0.9	0.0308
382	0.9	0.9	0.0298
383	0.3	0.95	0.0313
384	0.5	0.95	0.0315
385	0.9	0.95	0.0330

OMS Pod				
T/C	XO, in.	YO, in.	ZO, in.	b, in.
1D	1312.5	103.47	437.62	0.039
2D	1312.5	105.65	451.57	0.025
3D	1313.4	99.92	463.35	0.041
4D	1314.2	90.04	474.41	0.043
5D	1315.4	81.42	485.17	0.028
6D	1316.2	69.87	492.67	0 027
7D	1317.8	56.21	497.18	0.027
8D	1319.2	42.82	495.98	0.031
9D	1322.7	113.14	434.29	0.023
10D	1322.9	113.90	446.10	0.033
11D	1323.2	115.62	459.73	0.029
12D	1323.4	110.38	472.01	0.036
13D	1324.9	101.55	482.44	0.031
14D	1326.3	92.10	492.89	0.024
15D	1327.3	80.93	501.43	0.026
16D	1328.5	68.91	508.10	0.029
17D	1331.3	54.30	510.38	0.029
18D	1332.4	41.74	504.13	0.028
19D	1336.5	114.14	437.45	0.027
20D	1336.1	120.76	449.86	0.034
21D	1336.0	124.01	462.41	0.026
22D	1335.5	119.09	475.11	0.028
23D	1336.8	110.33	485.84	0.030
24D	1337.4	93.43	495 69	0.029
25D	1338.4	83.08	504.61	0.031

OMS Pod				
T/C	XO, in.	YO, in	ZO, in.	b, in
26D	1339.9	76.58	512.79	0.030
27D	1341.3	64.09	517.49	0.026
28D	1343.2	50.13	514.51	0.030
29D	1344.8	38.66	506.42	0.029
30D	1348.9	111.89	427.05	0.015
31D	1348.0	119.71	438.95	0.023
32D	1346.9	126.40	451.59	0.029
33D *	1346.9	128.97	464.66	0.027
34D	1347.9	123.26	478.95	0.029
35D	1348.6	114.89	488.55	0.031
36D	1350.0	104.37	498 45	0.031
37D	1350.9	93.15	507.16	0.032
38D	1351.9	81.63	515.29	0.031
39D	1353.3	68.97	521.19	0.029
40D	1355.5	55.02	520 43	0.033
41D	1356.8	42.64	512.69	0.028
42D	1360.9	115.72	428.93	0.016
43D	1360.7	124.34	441.15	0.023
44D	1359.7	130.58	452.74	0.032
45D	1359.5	133.68	466.33	0.033
46D	1359.8	128.57	479.54	0.031
47D	1360.0	119.66	489.71	0.029
48D	1361.1	109.53	499.35	0.026
49D	1362.4	98.70	508.42	0.027
50D	1363.8	86.87	516.86	0.029

* NO DATA ON TUNNEL TAPE

TABLE IV. (Continued)

OMS Pod				
T/C	XO, in.	YO, in.	ZO, in.	b, in.
51D	1365.3	74.61	524.20	0.030
52D	1367.4	60.48	524.50	0.034
53D	1369.0	48.26	518.62	0.030
54D	1370.3	36.90	508.92	0.027
55D	1373.1	120.67	431.05	0.019
56D	1372.1	128.48	442.97	0.024
57D	1371.2	134.78	454.73	0.033
58D	1371.1	137.31	467.72	0.037
59D	1372.0	132.02	481.22	0.034
60D	1372.9	122.88	491.72	0.032
61D	1373.7	112.41	501.33	0.029
62D	1375.3	100.96	510.86	0.026
63D	1376.4	89.49	519.21	0.024
64D	1378.0	77.00	525.93	0.032
65D	1379.7	63.26	527.07	0.036
66D	1380.8	50.74	521.79	0.029
67D	1382.4	38.65	512.32	0.027
68D	1385.9	115.78	421.02	0.020
69D	1385.6	123.25	431.09	0.020
70D	1383.9	131.73	443.72	0.025
71D	1383.9	137.99	455.55	0.031
72D	1383.3	140.31	469.43	0.036
73D	1383.3	134.47	482.98	0.033
74D	1384.2	125.46	493.31	0.031
75D	1385.5	114.84	503.23	0.026

OMS Pod				
T/C	XO, in.	YO, in.	ZO, in	b, in.
76D	1386.9	104.23	511.85	0.025
77D	1396.2	140.63	456.75	0.034
78D	1395.7	142.72	471.17	0.040
79D	1395.4	137.55	483.60	0.035
80D	1407.8	143.07	458.22	0.035
81D	1408.2	144.85	472.53	0.040
82D	1408.3	138.82	486.10	0.035
83D	1420.6	145.46	460.82	0.035
84D	1420.3	146.41	474.10	0.040
85D	1420.7	140.53	487.50	0.034
86D	1433.1	147.19	461.84	0.034
87D	1432.7	147.95	474.38	0.038
88D	1433.3	142.34	488.33	0.031

Upper Wing			
T/C	$(X/C)_W$	2Y/B	b, in.
253	0.0250	0.6	0.009
254	0.050	0.6	0.0110
255	0.10	0.6	0.0210
256	0.20	0.6	0.0250
257	0.40	0.6	0.0270
258	0.60	0.6	0.0240
259	0.75	0.6	0.025
462	0.715	0.6	0.029
260	0.85	0.6	0.027
261	0.95	0.6	0.02
463	0.7	0.65	0.029
262	0.2	0.7	0.024
263	0.4	0.7	0.025
476	0.6	0.7	0.030
464	0.69	0.7	0.030
264	0.9	0.7	0.0280
465	0.68	0.725	0.029
265	0.10	0.75	0.023
266	0.20	0.75	0.023
267	0.40	0.75	0.025
477	0.5	0.75	0.028
268	0.60	0.75	0.022
466	0.67	0.75	0.027
269	0.8	0.75	0.024
270	0.9	0.75	0.028

Upper Wing			
T/C	$(X/C)_W$	2Y/B	b, in.
467	0.66	0.775	0.024
478	0.1	0.8	0.031
479	0.3	0.8	0.032
480	0.4	0.8	0.032
481	0.5	0.8	0.032
468	0.65	0.8	0.024
482	0.725	0.8	0.025
469	0.64	0.825	0.024
483	0.715	0.825	0.028
484	0.85	0.825	0.025
485	0.90	0.825	0.029
486	0.1	0.85	0.032
487	0.2	0.85	0.030
488	0.4	0.85	0.030
489	0.5	0.85	0.030
470	0.63	0.85	0.025
490	0.7	0.85	0.029
471	0.62	0.875	0.026
272	0.2	0.9	0.025
273	0.4	0.9	0.025
274	0.6	0.9	0.03
472	0.575	0.925	0.027
275	0.2	0.95	0.023
276	0.4	0.95	0.03
277	0.95	0.95	0.025

TABLE IV. (Concluded)

Upper Wing			
T/C	$(X/C)_W$	2Y/B	b, in.
278	0.7	0.95	0.028
279	0.8	0.95	0.029
280	0.9	0.95	0.028
473	0.45	0.975	0.020

Upper Fuselage			
T/C	X/L	PHI, deg	b, in.
183	0.45	180	0.026
185	0.55	180	0.026
186	0.60	180	0.025
187	0.65	180	0.024
188	0.70	180	0.025
189	0.75	180	0.0255
223	0.40	157.5	0.034
224	0.45	157.5	0.034
225	0.50	157.5	0.034
226	0.55	157.5	0.035
227	0.60	157.5	0.034
228	0.65	157.5	0.0325
230	0.75	157.5	0.03
231	0.80	157.5	0.032
234	0.40	135.0	0.03
235	0.45	135.0	0.03
236	0.50	135.0	0.036
237	0.55	135	0.035
238	0.6	135	0.031
240	0.7	135	0.03
241	0.75	135	0.32
242	0.8	135	0.32
389	0.45	114	0.033
390	0.50	114	0.036
391	0.55	114	0.0345

Upper Fuselage			
T/C	X/L	PHI, deg	b, in.
392	0.6	114	0.0335
393	0.65	114	0.0345
394	0.70	114	0.034
395	0.75	114	0.036
T/C	X/L	Y, in.	b, in.
124A	0.3974	1.128	0.0308
125A	0.3961	0.868	0.029
126A	0.3974	0.560	0.0285
139A	0.496	1.564	0.0337
140A	0.496	0.868	0.0291
404A	0.595	1.572	0.0301
405A	0.594	1.12	0.0322
406A	0.595	0.868	0.0285
407A	0.595	0.560	0.0284
408A	0.595	0.280	0.026
410A	0.695	1.572	0.0334
155A	0.79	1.572	0.0307
156A	0.79	0.808	0.0264
158A	0.819	1.218	0.0248
159A	0.819	0.868	0.0264
160A	0.819	0.308	0.0306
36A	0.817	0.0140	0.0278

Forward Fuselage Side			
T/C	X/L	ZO, in	b, in.
210	0.1	410.0	0.037
220C	0.2	410.0	0.031
T/C	X/L	Y, in.	b, in.
89A	0.248	1.709	0.031
88A	0.247	.672	0.026
102A	0.296	1.638	0.023
103A	0.296	0.867	0.015
T/C	X/L	Z, in.	b, in.
205	0.05	378 4	0.033
206	0.076	350.0	0.035

Note: In the tabulated data, thermocouple numbers ending in A or C appear instead as 2000 or 1000 series numbers, respectively.

TABLE V. 56-0 Model Thermocouple Locations

Fuselage Side			
T/C	X/L	ZO	b, in.
1	.275	437.5	.0215
2	.300	442.0	.0210
3	.325	445.0	.0217
4	.350	445.0	.0215
5	.375	445.0	.0212
6	.400	445.0	.0217
7	.425	445.0	.0215
8	.450	445.0	.0218
9	.475	445.0	.0219
10	.500	445.0	.0220
11	.525	445.0	.0220
12	.550	445.0	.0222
13	.600	445.0	.0220
14	.650	445.0	.0220
15	.700	445.0	.0228
16	.750	445.0	.0220
17	.800	445.0	.0230
18	.285	420.0	.0190
19	.337	420.0	.0189
20	.390	420.0	.0189
21	.426	420.0	.0190
22	.478	420.0	.020
23	.530	420.0	.020
24	.567	420.0	.0205
25	.620	420.0	.0205

Fuselage Side			
T/C	X/L	ZO	b, in.
26	.670	420.0	.0205
27	.705	420.0	.0207
28	.750	420.0	.0203
29	.800	420.0	.0202
30	.824	420.0	.0160
31	.200	400.0	.0210
32	.225	400.0	.0199
33	.250	400.0	.0199
34	.275	400.0	.0186
35	.300	400.0	.0180
36	.325	400.0	.0190
37	.350	400.0	.0192
38	.375	400.0	.0190
39	.400	400.0	.0189
40	.425	400.0	.0188
41	.450	400.0	.0195
42	.475	400.0	.0200
43	.500	400.0	.0200
44	.525	400.0	.0190
45	.550	400.0	.0200
46	.600	400.0	.0205
47	.650	400.0	.0210
48	.700	400.0	.0202
49	.750	400.0	.0205
50	.800	400.0	.0208

Fuselage Side			
T/C	X/L	ZO	b, in.
51	.850	400.0	.0180
52	.875	400.0	.0180
53	.900	400.0	.0160
54	.925	400.0	.0170
55	.950	400.0	.0220
56	.300	372.5	.0170
57	.325	372.5	.0170
58	.350	372.5	.0170
59	.375	372.5	.0170
60	.400	372.5	.0170
61	.425	372.5	.0170
62	.450	372.5	.0172
63	.475	372.5	.0175
64	.500	372.5	.0180
65	.525	372.5	.0180
66	.550	372.5	.0190
67	.600	372.5	.0193
68	.650	372.5	.0190
69	.700	327.2	.0200
70	.750	372.5	.0200
71	.200	355	.0195
72	.225	355	.0190
73	.250	355	.0190
74	.275	355	.0180
75	.800	355	.0185

Fuselage Side			
T/C	X/L	ZO	b, in.
76	.850	355	.0188
77	.875	355	.0170
78	.900	355	.0172
79	.925	355	.0180
80	.950	355	.0190

TABLE VI. 83-0 Model Thermocouple Locations

Canopy			
T/C	RAY	LINE	b, in.
177	1	4	.0308
178	1	6	.0440
179	2	6	.0469
180	3	3	.0292
181	3	4	.0304
182	3	5	.0319
183	4	1	.0281
184	4	2	.0306
185	4	3	.0269
186	4	4	.0281
187	4	5	.0298
188	4	6	.0592
189	5	3	.0319
190	5	4	.0322
191	5	5	.0342
192	6	2	.0316
193	6	6	.0431
194	7	3	.0289
195	7	4	.0276
196	7	5	.0294
197	8	1	.0222
198	8	2	.0260
199	8	3	.0301
200	8	4	.0319
201	8	5	.0316

Canopy			
T/C	RAY	LINE	b, in.
202	8	6	.0283
203	9	3	.0278
204	9	4	.0348
205	9	5	.0349
206	10	2	.0297
207	10	6	.0300
208	11	3	.0301
209	11	4	.0308
210	11	5	.0299
212	12	2	.0302
213	12	3	.0297
211	12	1	.0279
216	12	6	.0318
217	12	7	.0319
218	13	3	.0309
219	13	4	.0315
220	13	5	.0308
222	14	2	.0276
223	14	6	.0304

Upper Centerline			
T/C	X/L	PHI	b, in.
398	.1519	180	.0315
399	.1556	180	.0299
400	.1582	180	.0302
401	.1608	180	.0290
414	.2049	180	.0300
403	.1664	180	.0272
404	.1691	180	.0271
406	.1748	180	.0271
407	.1769	180	.0289
408	.1800	180	.0328
416	.250	180	.0262
411	.1894	180	.0336
412	.1931	180	.0312
413	.1972	180	.0300

Right Side			
T/C	X/L	ZO	b, in.
311	.20	355	.023
312	.225	355	.025
313	.250	355	.0296
314	.275	355	.0279
315	.300	355	.0308
319	.400	355	.0278
317	.350	355	.0311
318	.375	355	.0302
323	.200	378	.0259

Right Side			
T/C	X/L	ZO	b, in.
324	.225	378	.0368
355	.150		.0273
326	.275	378	0261
327	.300	378	.0286
328	.325	378	.0249
329	.350	378	.0306
330	.375	378	.0282
331	.400	378	.0269
357	.200		.0262
334	.225	400	.0255
335	.250	400	.0289
336	.275	400	.0262
337	.300	400	.0303
338	.325	400	.0269
339	.350	400	.0302
356	.175		.0311
341	.400	400	.0279
344	.325	425	.031
345	.350	425	.030
346	.375	425	.030
347	.400	425	.030
358	.275		.032
359	.300		.0310
360	325		.030
361	.350		.0305
362	.375		.030
364	.425		.032

TABLE VII

PHASE CHANGE PAINT TEST DATA SUMMARY

TEST OH109B

ALPHA, DEG	YAW, DEG	REx10^{-6}, ft^{-1}	PHASE CHANGE PAINT TEMPERATURE, ^{o}F						
			250	300	350	450	550	600	700
35	0	0.6		317					
35	-2	↓		318					
35	0	1.0			309				
35	-2	↓			314				
40	0	↓	311	313	310				
40	-2	↓		312					
30	0	2.0						305	
35	0	↓					306		
40	0	↓				308	307		
30	0	3.0							300
30	-2	↓							304
35	0	↓						302	301
35	-2	↓						303	
30	0	3.7			292	293	294		295
30	-2	↓							299
35	0	↓							296,297
35	-2	↓							298

Deleted: RUNS 315 and 316

TABLE VIII. BAD THERMOCOUPLES

(1) LISTING OF MODEL (60-0) BAD THERMOCOUPLES:

Thermocouple No.	Location	Remarks
346	Vertical Tail	Bad
353		Open
355		Open
360		Bad
371		Short
380	Vertical Tail	Can't Find (Lost ID)
33D	OMS Pod	Bad
62D		Open
66D		Open
69D	OMS Pod	Bad
182	Upper Fuselage	Bad
184		Open
190		Open
229		Open
239		Bad
396		Can't Find (Lost ID)
127A		Open
157A	Upper Fuselage	Bad
219	FWD Side Fuselage	Bad
87A		Can't Find (Lost ID)

The following thermocouples were bad during runs 1-54:

256	Upper Wing	Bad
259		
273		
275		
279		

(2) LISTING OF MODEL (83-0) BAD THERMOCOUPLES:

214	Canopy	Bad
215/225		Open
316/319	Right Side Fuselage	Bad
325		
330		
363		
402	Upper Canopy	Bad
405/415		
407		
409		
410		

TABLE IX

MODEL MATERIAL THERMOPHYSICAL PROPERTIES

Novamide 700-55

TPC, ^{o}F	$\sqrt{PCK}$, $Btu/ft^2\text{-}sec^{1/2}\text{-}^{o}R$
250	0.057
300	0.058
350	0.059
450	0.060
550	0.060
600	0.059
700	0.058

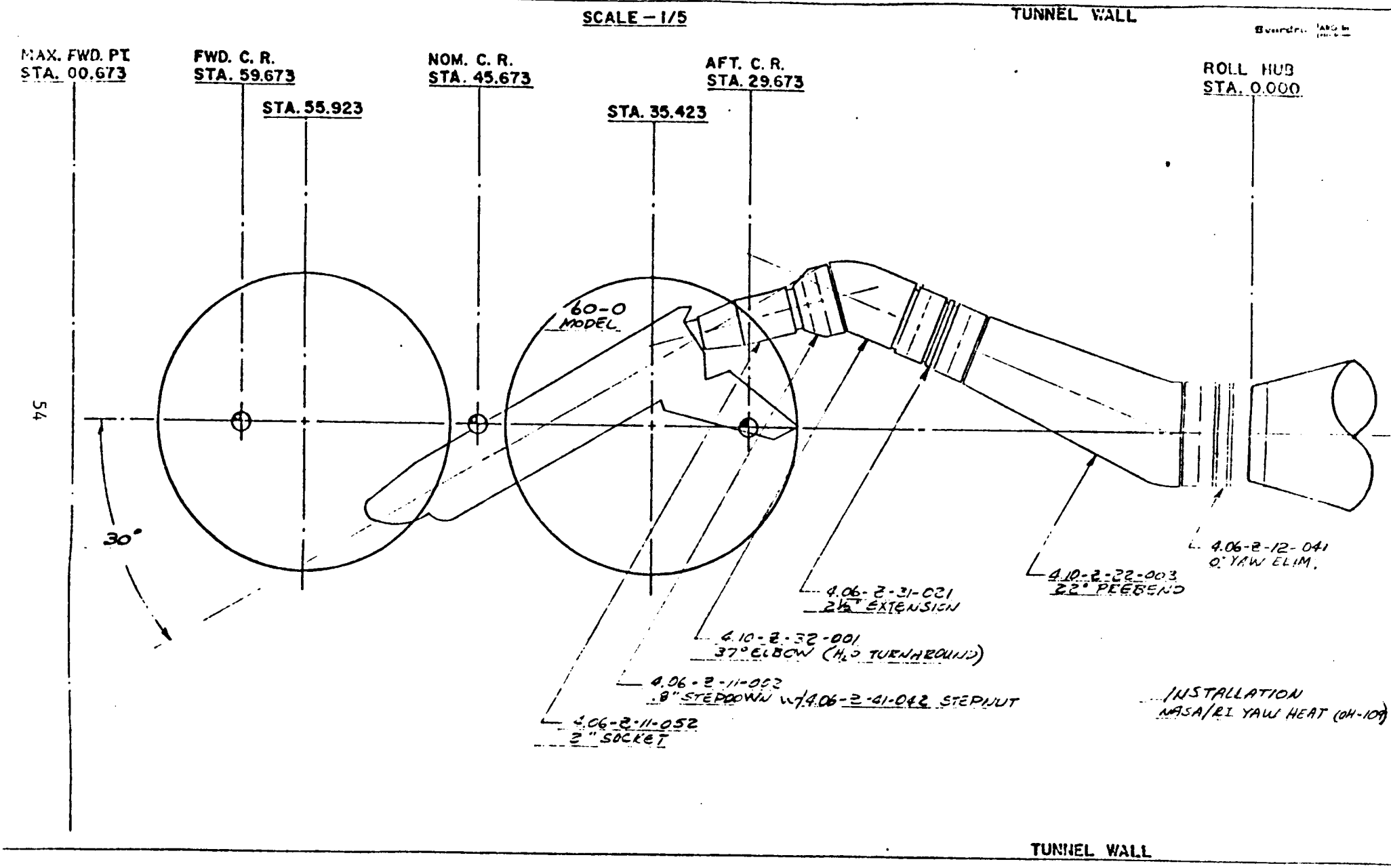

Fig. 1. 60-0 Model Installation

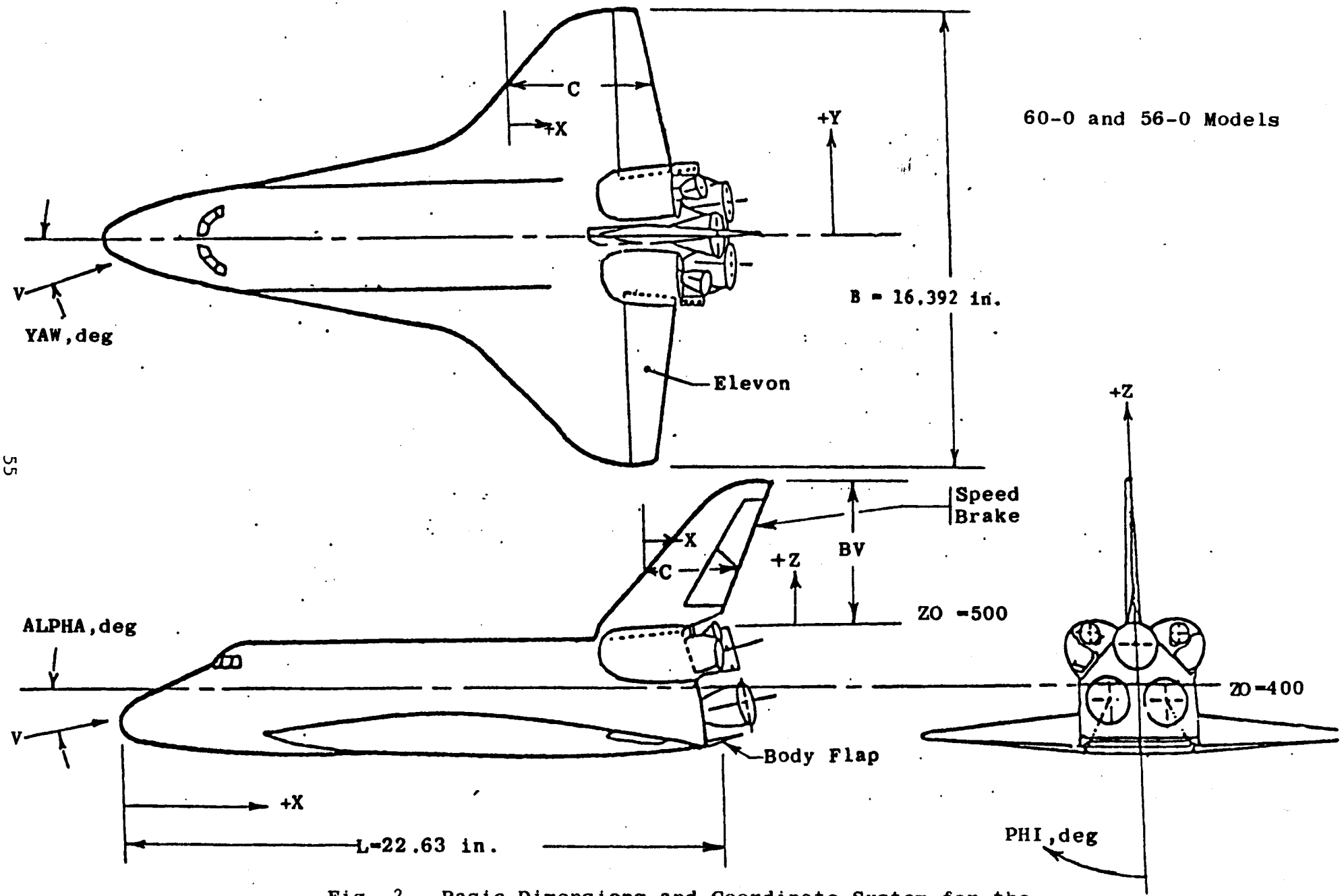

Fig. 2. Basic Dimensions and Coordinate System for the 0.0175 Scale Orbiter Models

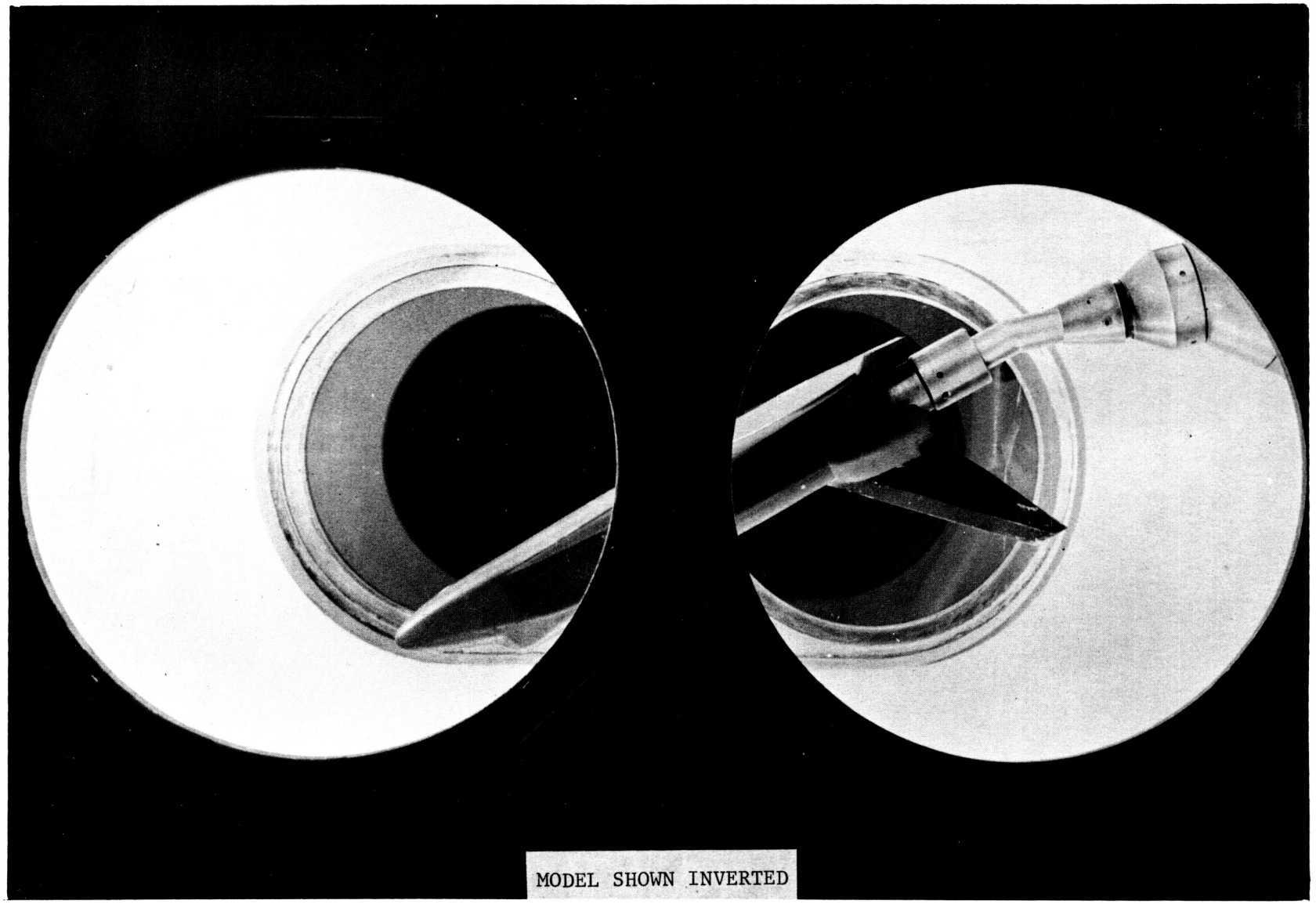

Fig. 3. Installation Photograph of 56-0 Model

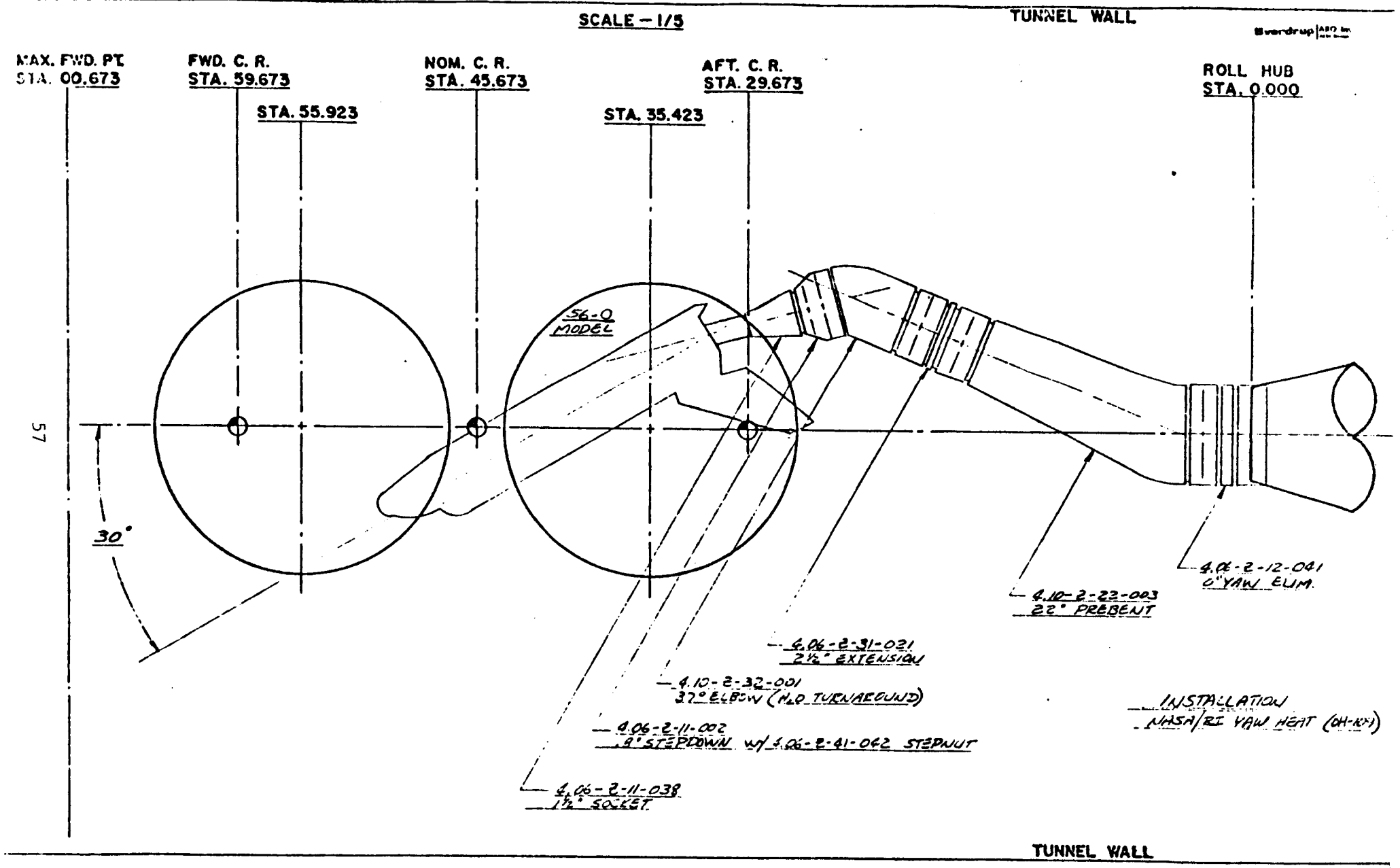

Fig. 4. 56-0 Model Installation for Thin-Skin Thermocouple Test

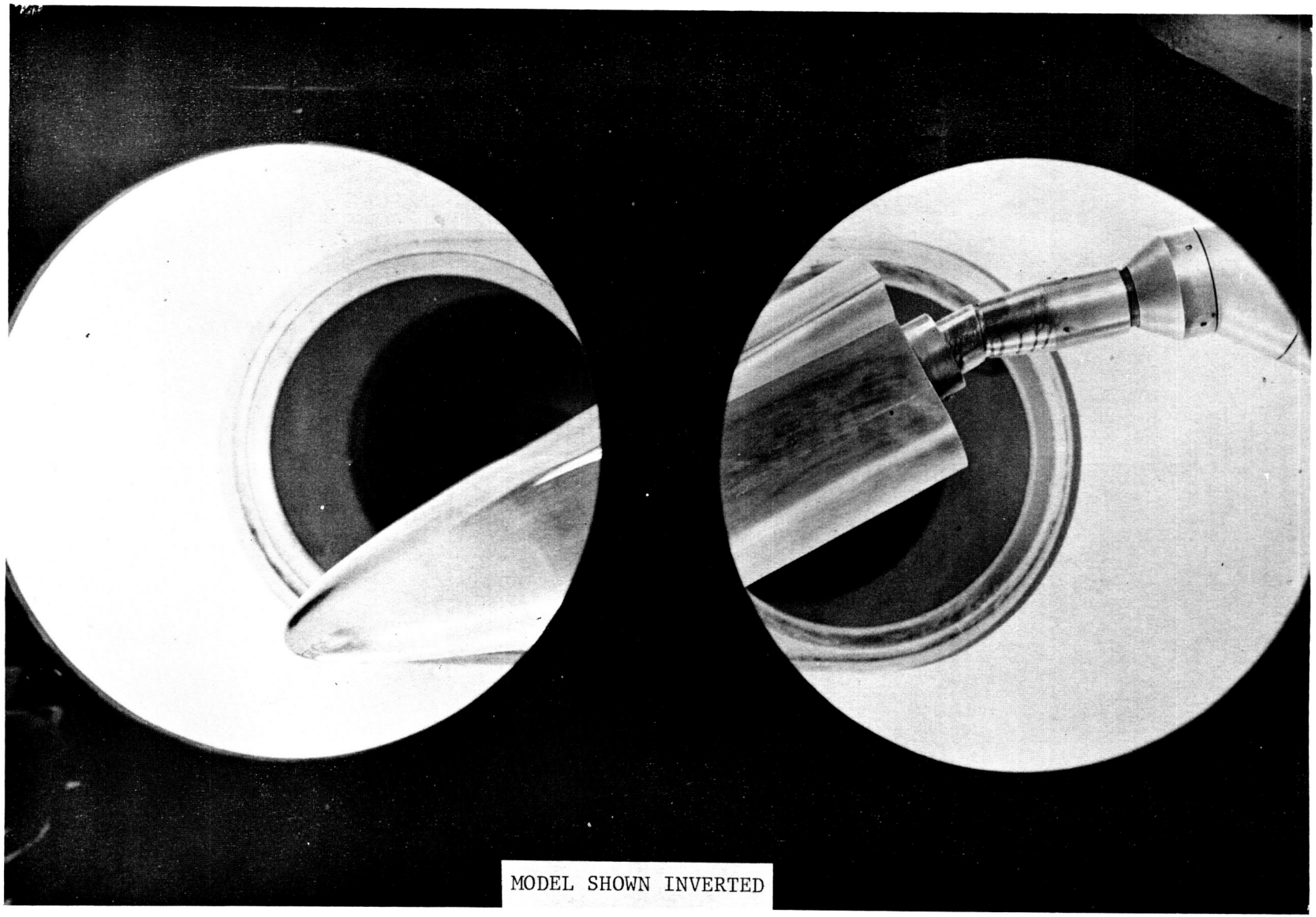

Fig. 5. Installation Photograph of 83-0 Model

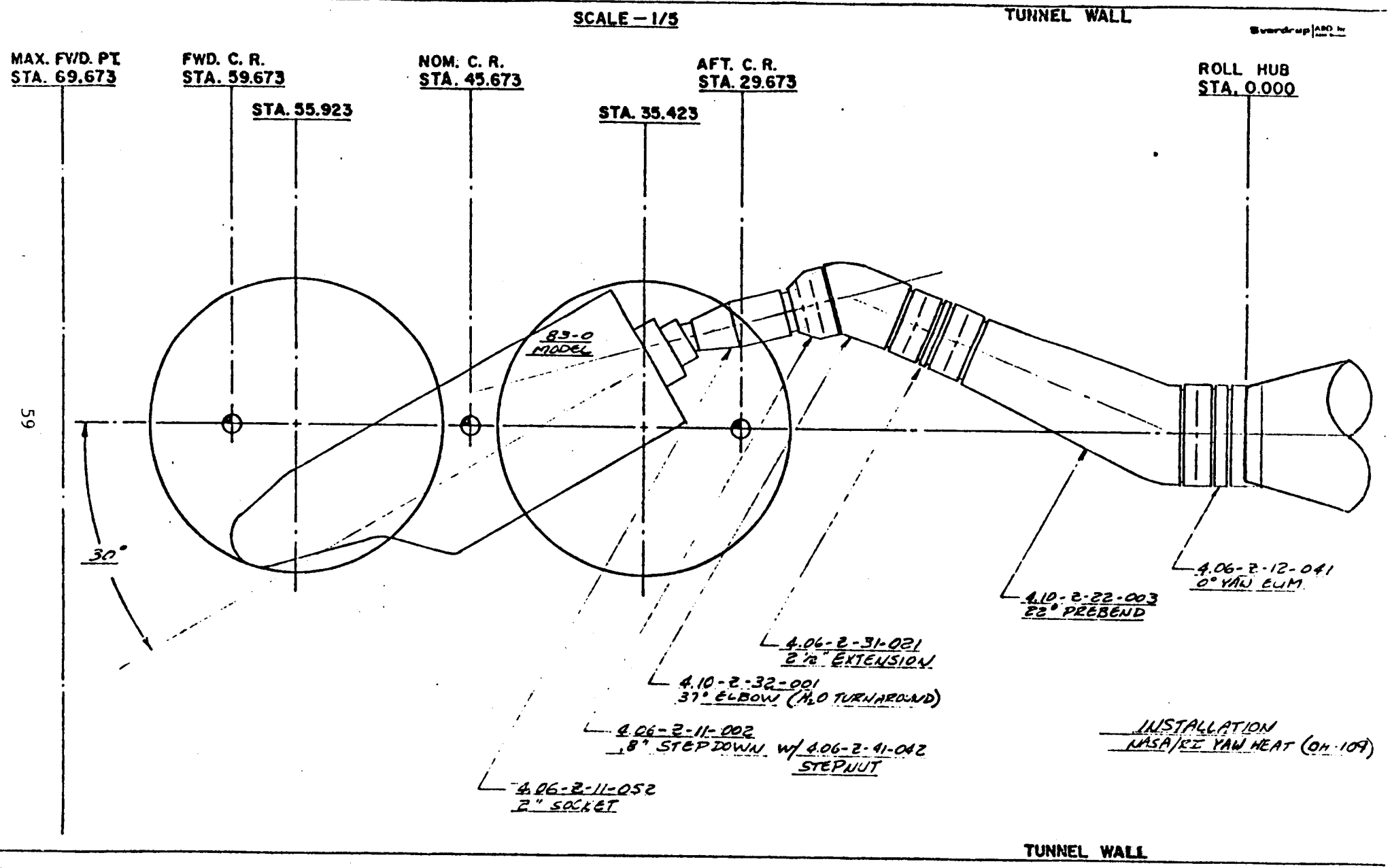

Fig. 6. 83-0 Model Installation

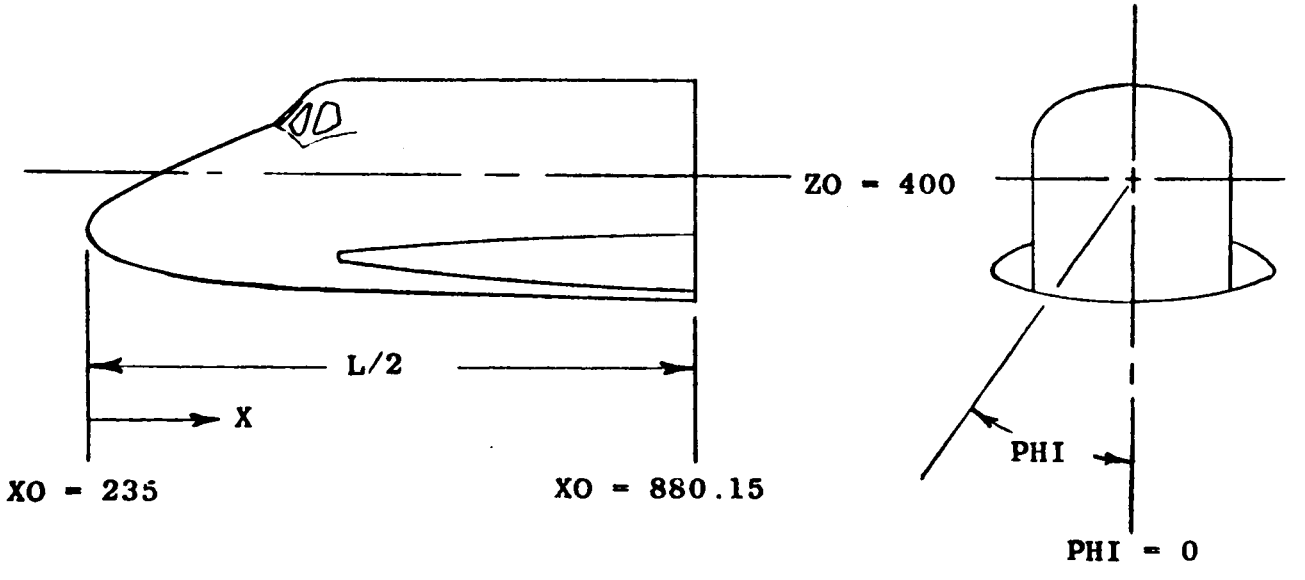

Fig. 7 . Basic Dimensions and Coordinate System for the 83-0 Model

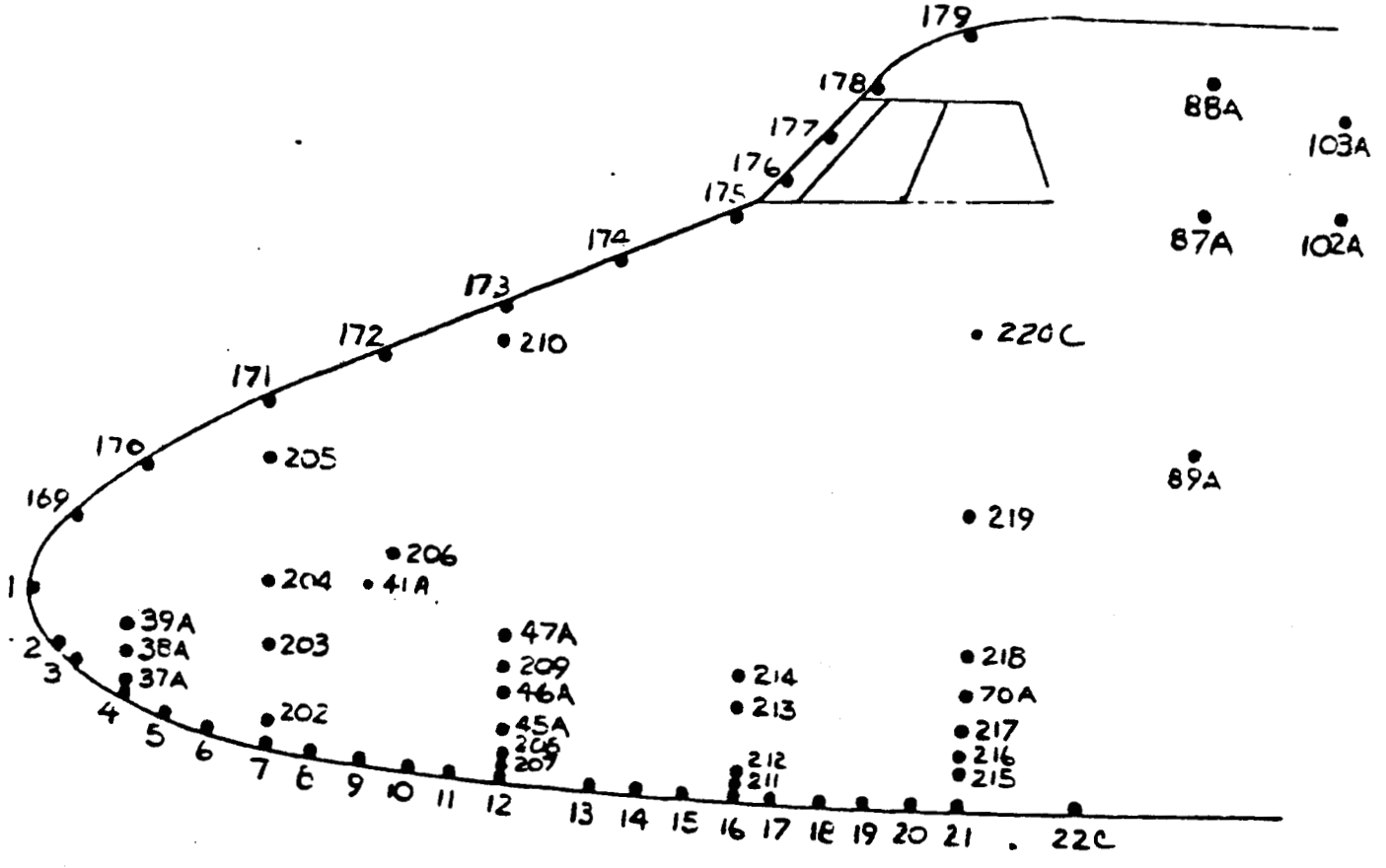

a. Nose and Canopy

Figure 8. Thermocouple Locations on the 60-Ø Model

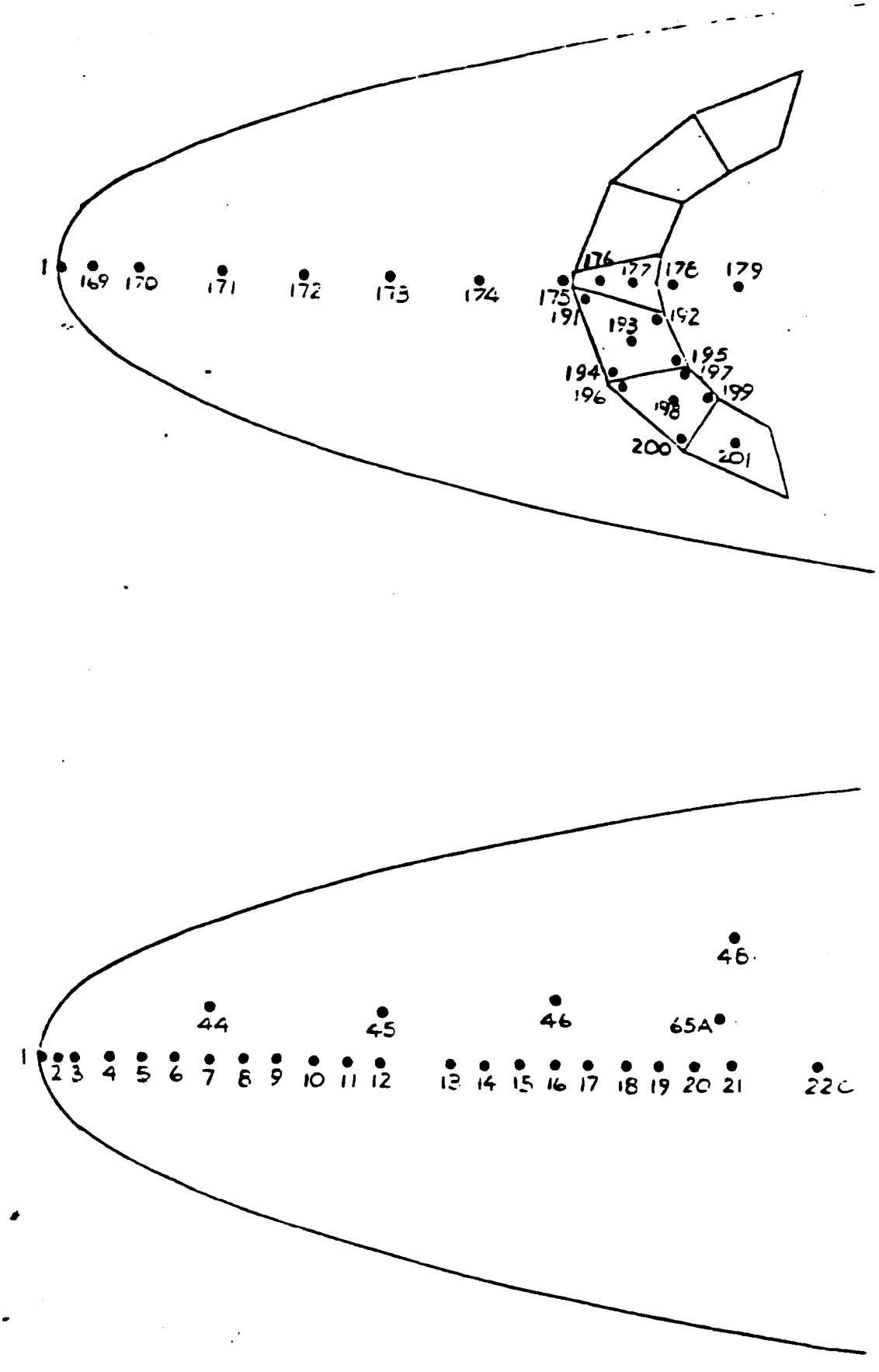

a. Nose and Canopy (Concluded)

Figure 8. Thermocouple Locations on the 60-Ø Model

(continued)

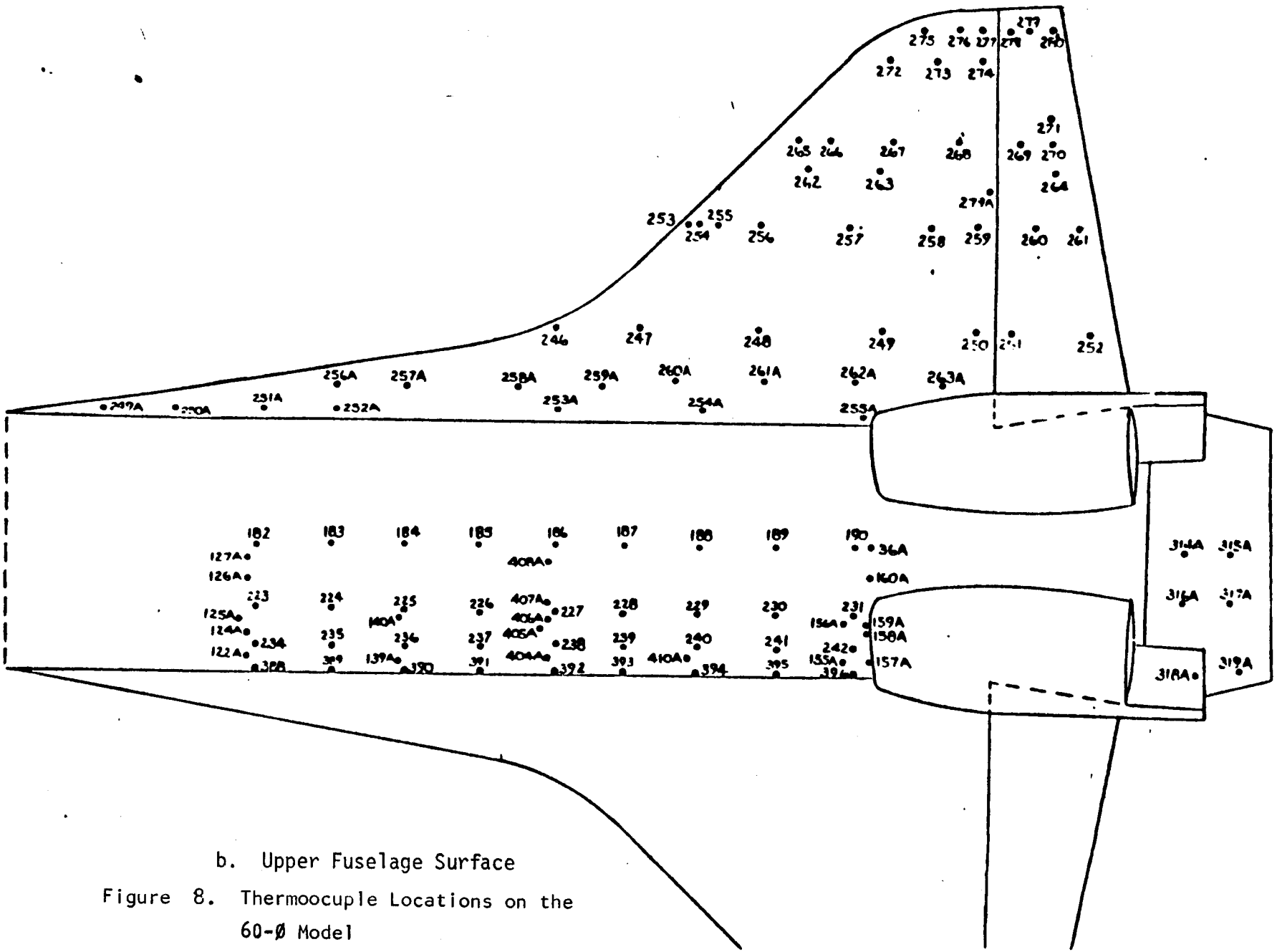

b. Upper Fuselage Surface

Figure 8. Thermoocuple Locations on the 60-Ø Model

(continued)

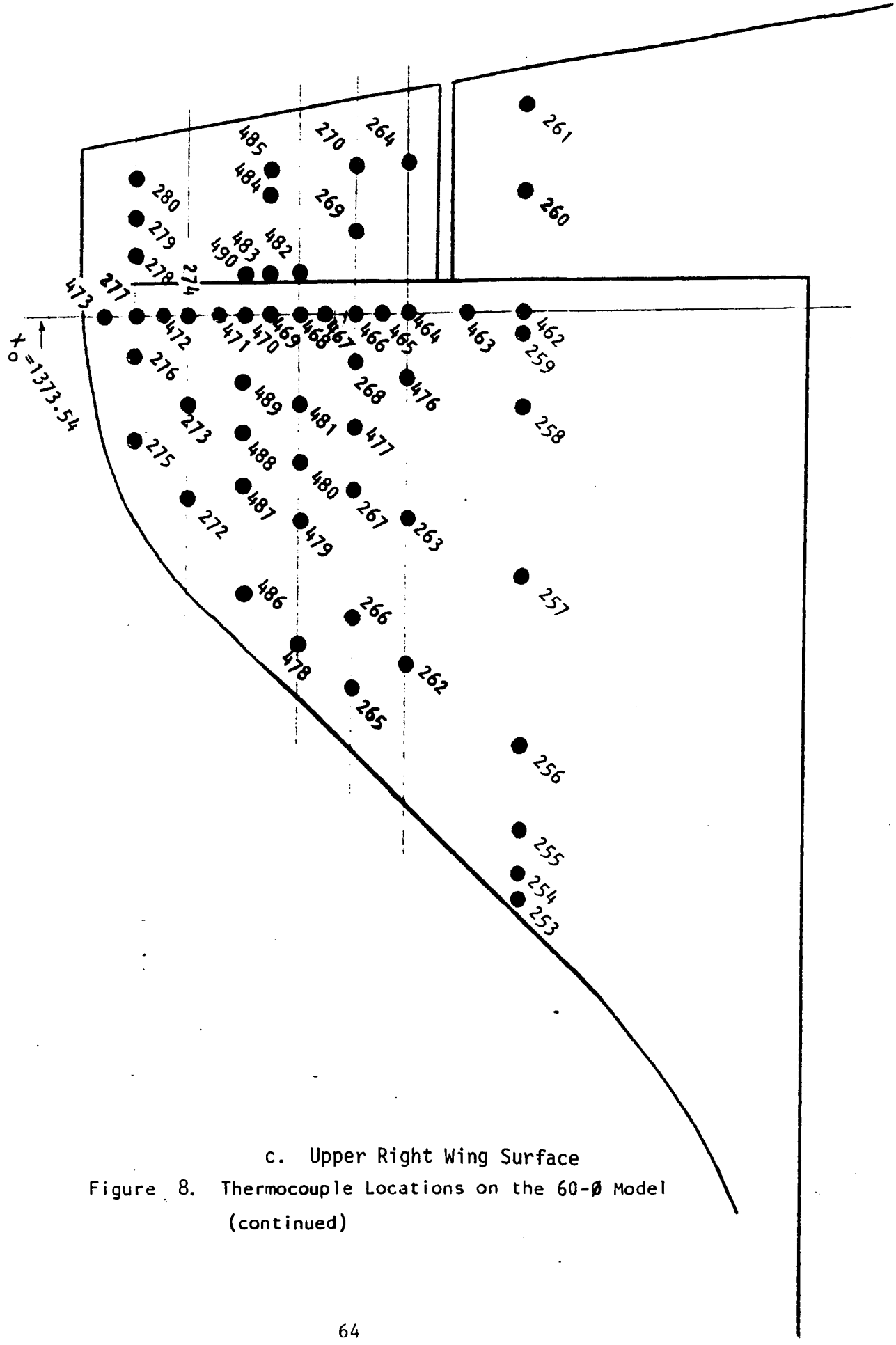

c. Upper Right Wing Surface

Figure 8. Thermocouple Locations on the 60-Ø Model (continued)

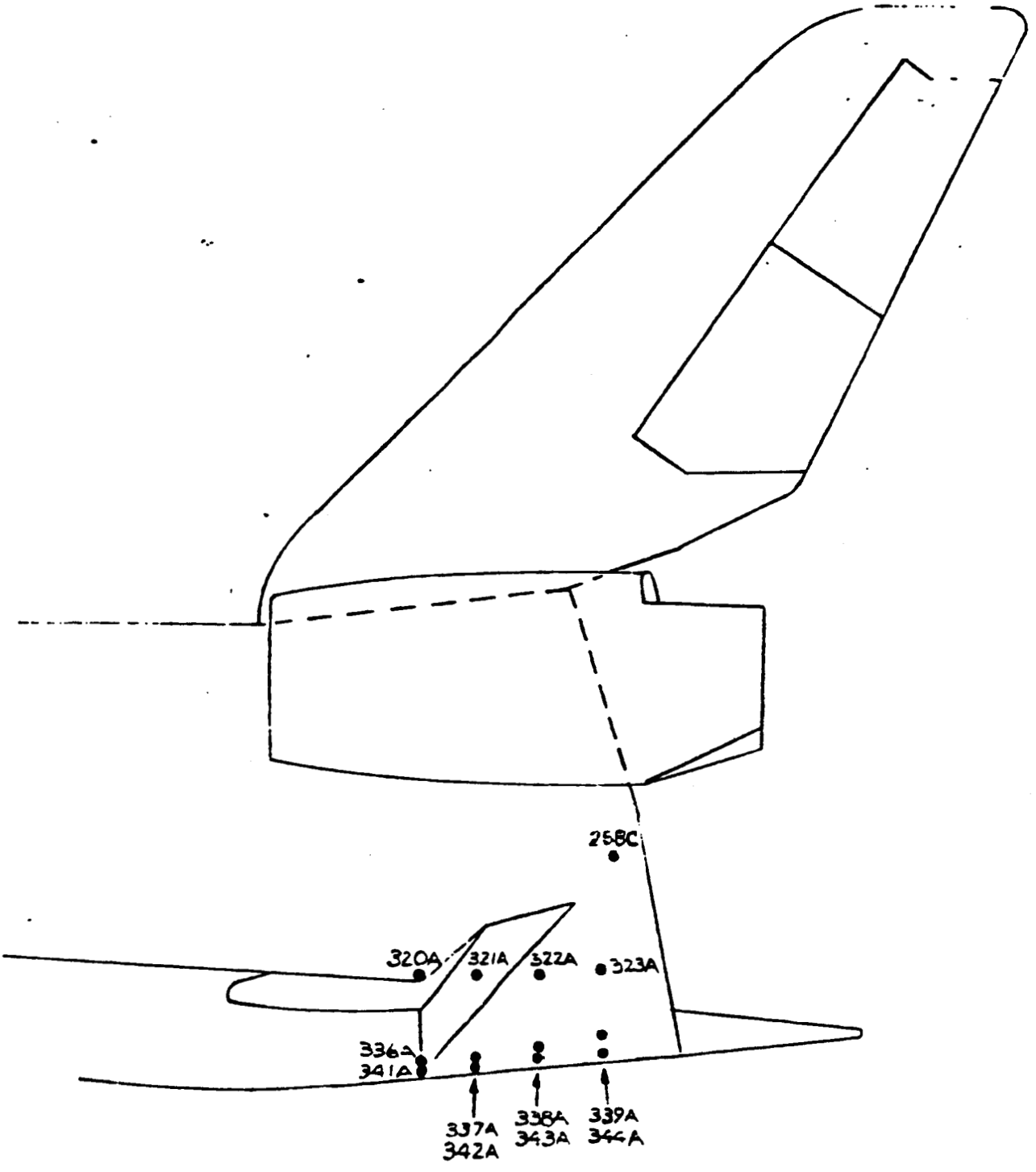

d. Aft Fuselage

Figure 8. Thermocouple Locations on the 60-Ø Model

(continued)

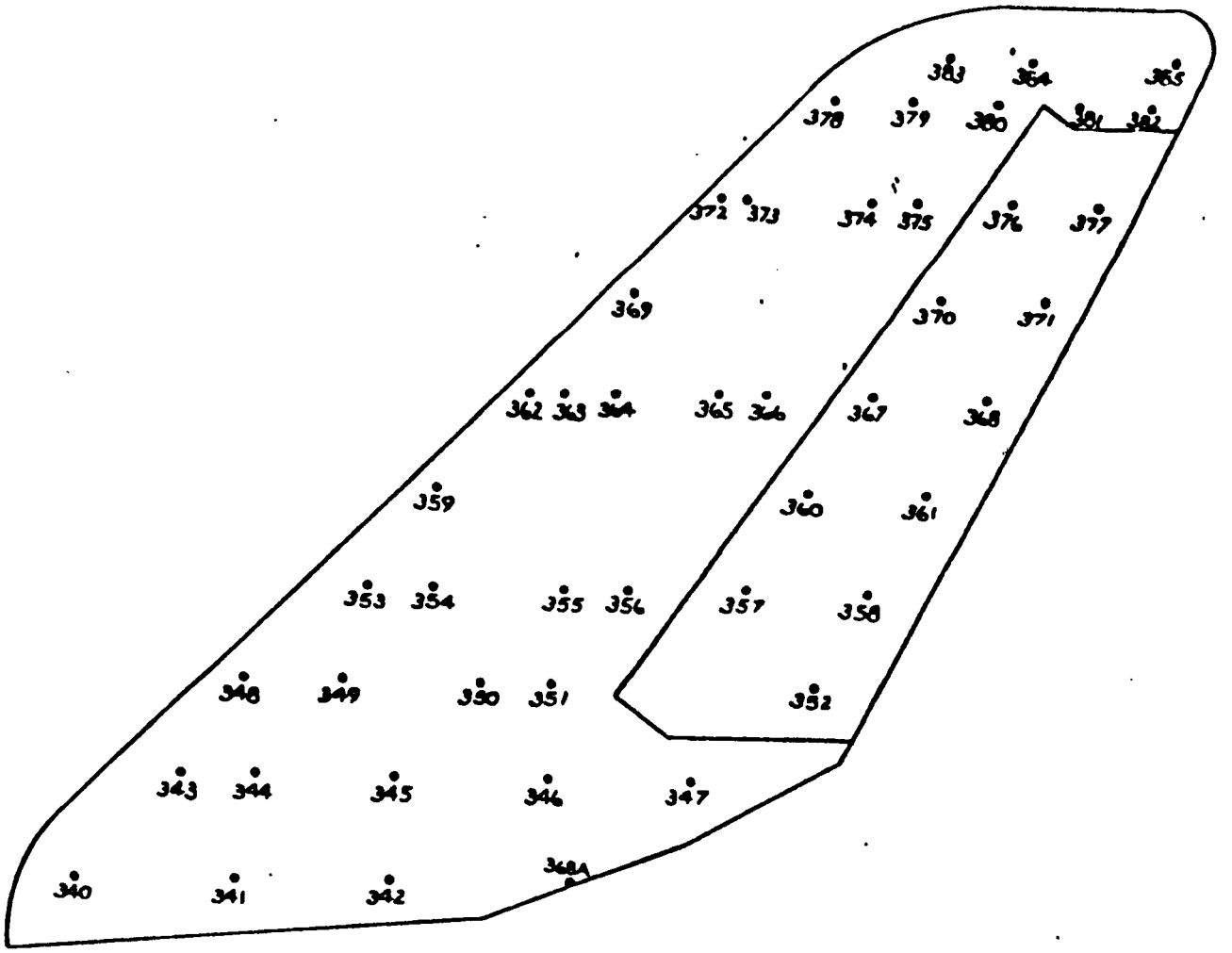

e. Vertical Tail Surface

Figure 8. Thermocouple Locations on the 60-Ø Model (continued)

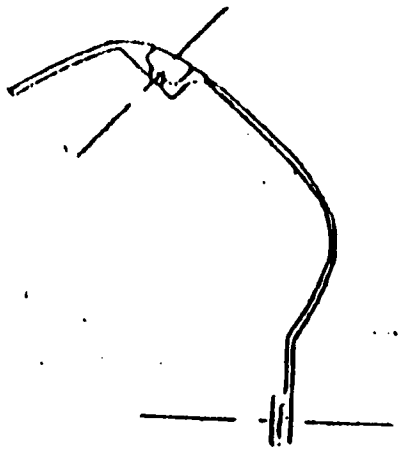

SECTION A-A.

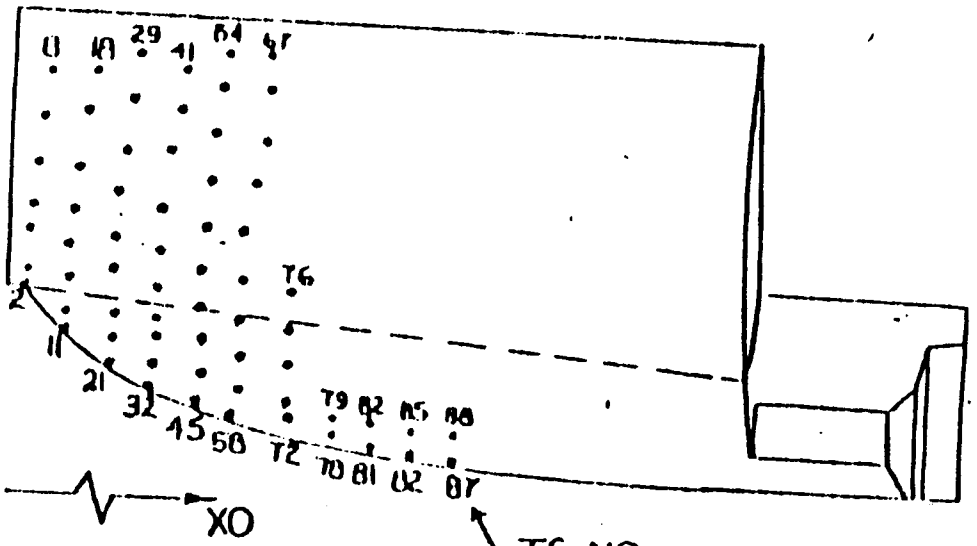

NOTE: FOR CLARITY, NOT ALL TC NO. SHOWN.

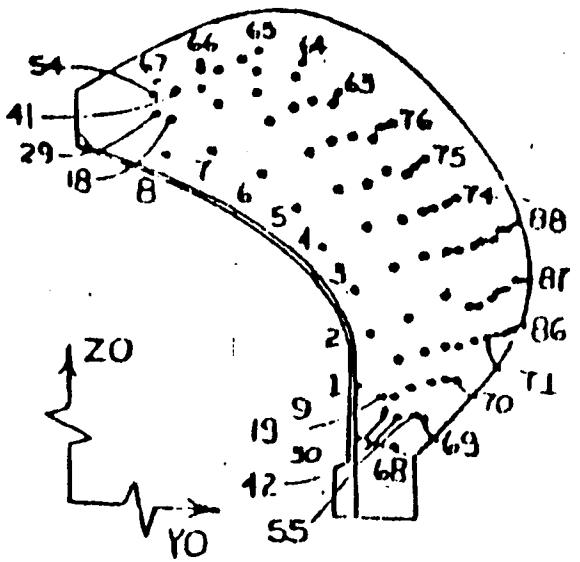

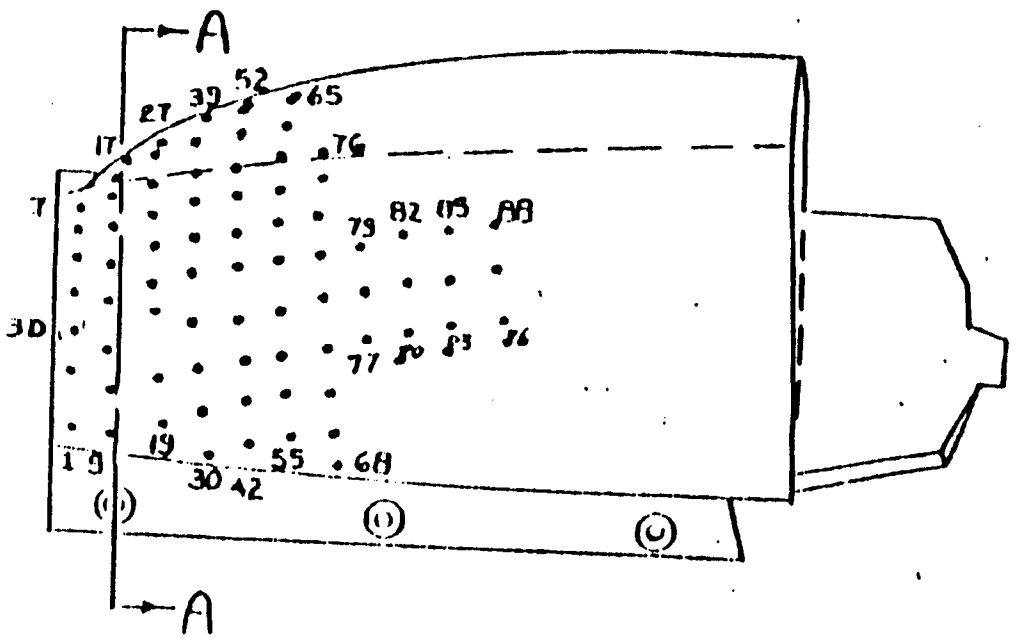

f. AFFDL Orbiter Maneuvering System (OMS) Pod
Figure 8. Thermocouple Locations on the 60-Ø Model (Concluded)

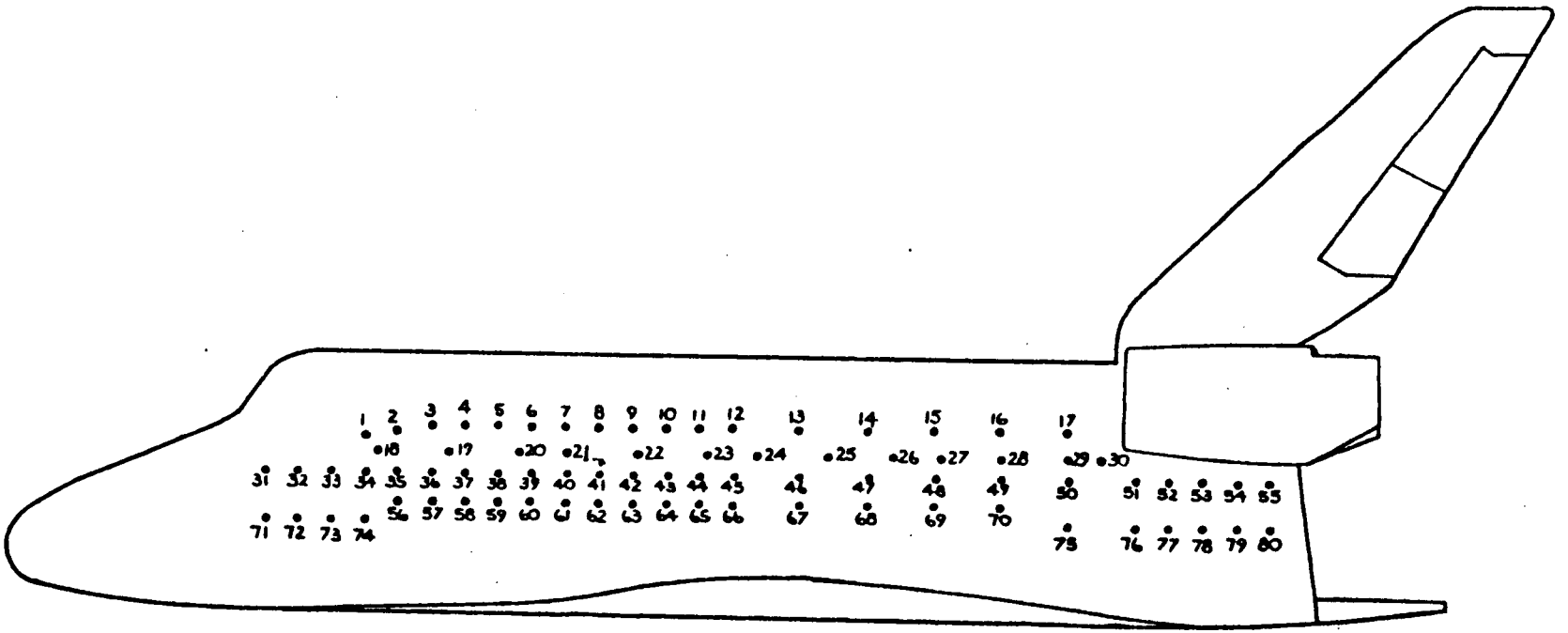

Fig. 9. Thermocouple Locations on 56-0 Model

MODEL 83-0

TEST OH109

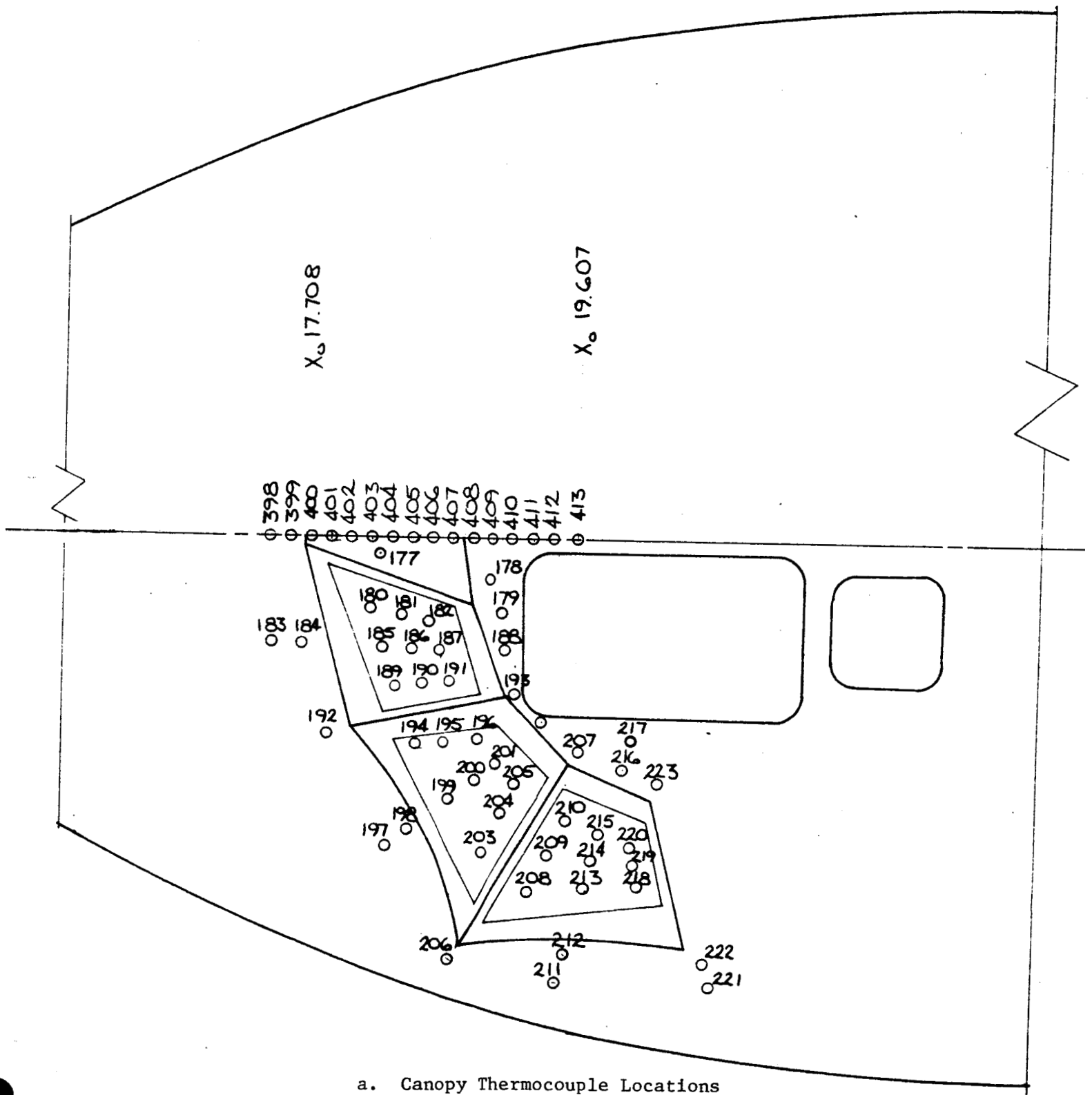

a. Canopy Thermocouple Locations

Figure 10. Thermocouple Locations on 83-0 Model

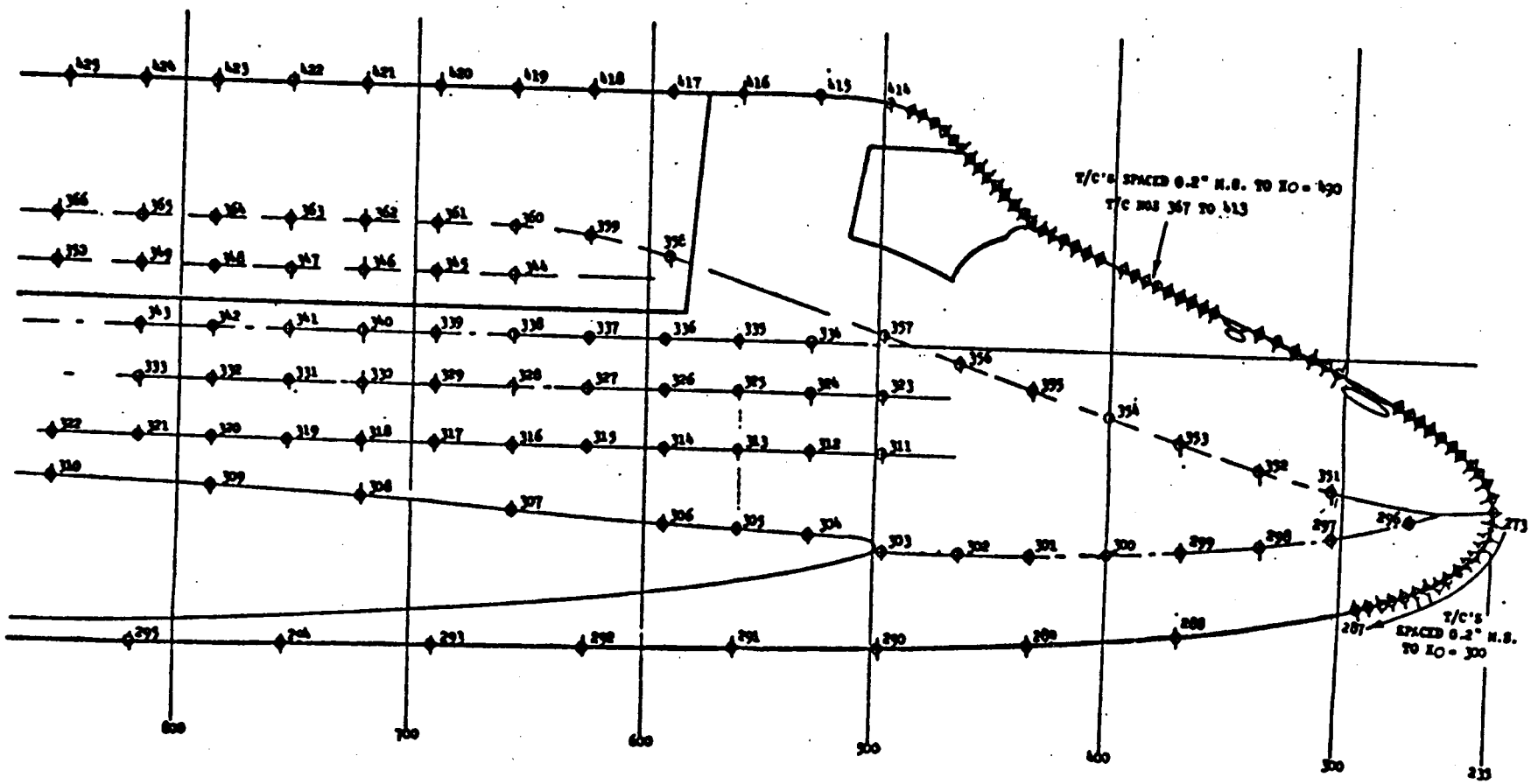

b. Thermocouple Locations on Fuselage Right Side

Fig. 10. Concluded

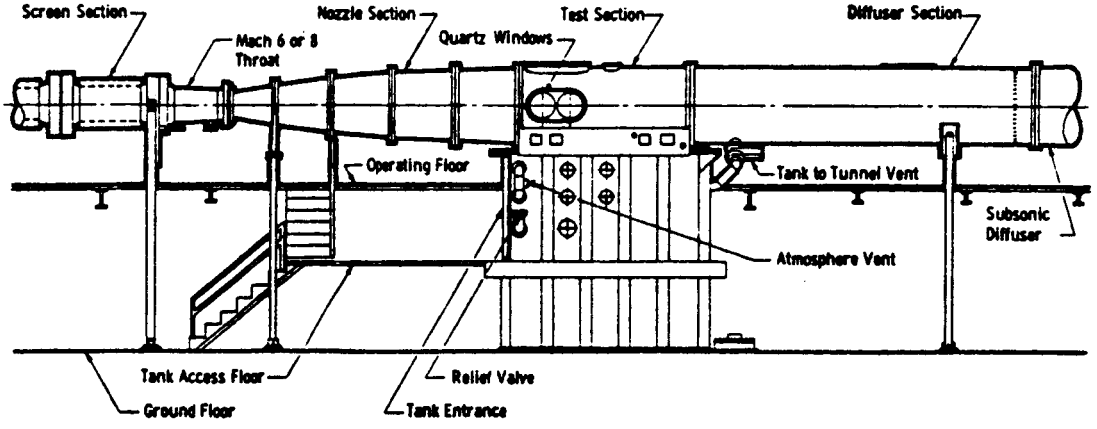

a. Tunnel assembly

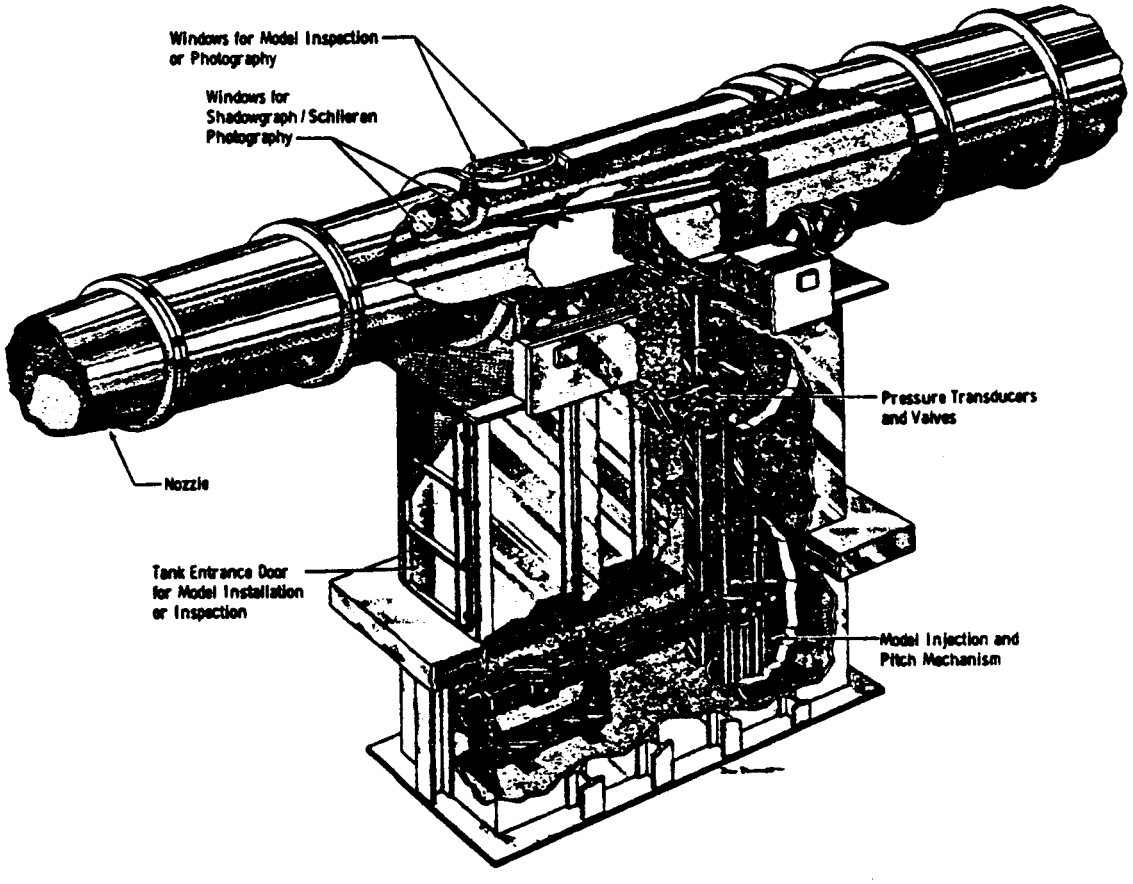

b. Tunnel test section

Figure 11. AEDC, VKF-Tunnel B

$$\text{Adjusted } H(TT) = \left[H(TT)_{\text{TAB DATA}} \right] \left[\frac{1}{\frac{H(TT)}{H(TRAX)}} \right]$$

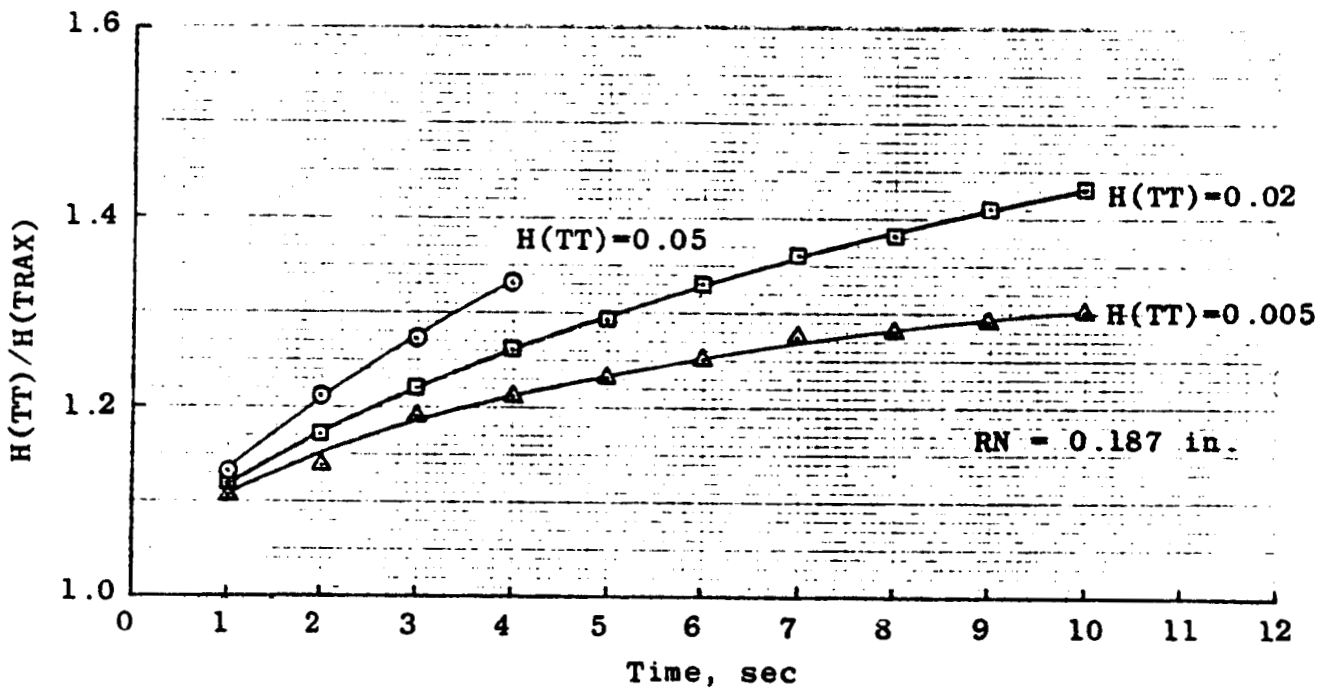

Fig. 12. Computed Influence of Semi-Infinite Slab Assumption on SILTS Pod Phase-Change Paint Data

Data Figures

(Microfiche Only)

(THIS PAGE INTENTIONALLY LEFT BLANK)